

Aura OMI observations of regional SO₂ and NO₂ pollution changes from 2005 to 2015

Nickolay A. Krotkov¹, Chris A. McLinden², Can Li^{3,1}, Lok N. Lamsal^{4,1}, Edward A. Celarier^{4,1}, Sergey V. Marchenko^{5,1}, William H. Swartz^{6,1}, Eric J. Bucsela⁷, Joanna Joiner¹, Bryan N. Duncan¹, K. Folkert Boersma^{8,9,10}, J. Pepijn Veefkind^{9,11}, Pieter F. Levelt^{9,11}, Vitali E. Fioletov², Russel R. Dickerson¹², Hao He¹², Zifeng Lu¹³, David G. Streets¹³

[1]{Atmospheric Chemistry and Dynamics Laboratory, NASA Goddard Space Flight Center, Greenbelt, Maryland, US }

[2]{Air Quality Research Division, Environment Canada, Toronto, Canada }

[3]{Earth System Science Interdisciplinary Center, University of Maryland, College Park, US }

[4]{GESTAR, Universities Space Research Association, Columbia, Maryland, US }

[5]{Science Systems and Applications, Inc., Lanham, Maryland, US }

[6]{Applied Physics Laboratory, Johns Hopkins University, Laurel, Maryland, US }

[7]{SRI International, Menlo Park, California, US }

[8]{Meteorology and Air Quality Group, Wageningen University, The Netherlands }

[9]{Royal Netherlands Meteorological Institute, De Bilt, The Netherlands }

[10]{Department of Applied Physics, Eindhoven University of Technology, Eindhoven, the Netherlands }

[11]{University of Technology Delft, Delft, the Netherlands }

[12]{Department of Atmospheric and Oceanic Science, University of Maryland, College Park, Maryland, USA }

[13]{Energy Systems Division, Argonne National Laboratory, Argonne, IL, USA }

Correspondence to: N. A. Krotkov (Nickolay.A.Krotkov@nasa.gov)

1 **Abstract**

2 The Ozone Monitoring Instrument (OMI) onboard NASA's Aura satellite has been providing
3 global observations of the ozone layer and key atmospheric pollutant gases, such as nitrogen
4 dioxide (NO₂) and sulfur dioxide (SO₂), since October 2004. The data products from the same
5 instrument provide consistent spatial and temporal coverage and permit the study of
6 anthropogenic and natural emissions on local-to-global scales. In this paper we examine changes
7 in SO₂ and NO₂ over some of the world's most polluted industrialized regions during the first
8 decade of OMI observations. In terms of regional pollution changes, we see both upward and
9 downward trends, sometimes in opposite directions for NO₂ and SO₂, for the different study
10 areas. The trends are, for the most part, associated with economic and/or technological changes
11 in energy use, as well as regional regulatory policies. Over the eastern US, both NO₂ and SO₂
12 levels decreased dramatically from 2005 to 2015, by more than 40% and 80%, respectively, as a
13 result of both technological improvements and stricter regulations of emissions. OMI confirmed
14 large reductions in SO₂ over eastern Europe's largest coal power plants after installation of flue
15 gas desulfurization devices. The North China Plain has the world's most severe SO₂ pollution,
16 but a decreasing trend has been observed since 2011, with about a 50% reduction in 2012-2015,
17 due to an economic slowdown and government efforts to restrain emissions from the power and
18 industrial sectors. In contrast, India's SO₂ and NO₂ levels from coal power plants and smelters
19 are growing at a fast pace, increasing by more than 100% and 50%, respectively, from 2005 to
20 2015. Several SO₂ hot spots observed over the Persian Gulf are probably related to oil and gas
21 operations and indicate a possible underestimation of emissions from these sources in bottom-up
22 emission inventories. Overall, OMI observations have proved to be very valuable in
23 documenting rapid changes in air quality over different parts of the world during the last decade.
24 The baseline established during the first 11 years of OMI is indispensable for the interpretation
25 of air quality measurements from current and future satellite atmospheric composition missions.

26 **1 Introduction**

27 Sulfur dioxide (SO₂) and nitrogen dioxide (NO₂) are reactive, short-lived atmospheric trace gases
28 with both anthropogenic and natural sources. Major sources of NO_x (NO_x =NO+NO₂) include
29 fossil fuel combustion, biomass burning, soil emissions (Vinken et al., 2014b), and lightning
30 (Schumann and Huntrieser, 2007). NO₂ participates in the nitrogen cascade of air – water – soil

1 (EPA, 2011; Galloway et al., 2013), affects atmospheric oxidation rates (Valin et al., 2013), and
2 contributes to surface ozone production (Duncan et al., 2010; Seinfeld and Pandis, 1998). The
3 principal sources of SO₂ are volcanic and anthropogenic emissions from burning sulfur-
4 contaminated fossil fuels and the refinement of sulfide ores. Volcanic SO₂ is often injected into
5 the atmosphere at high altitudes above the planetary boundary layer (PBL), while anthropogenic
6 SO₂ emissions are predominantly in or slightly above the PBL. Chemical reactions in the PBL
7 involving SO₂ and NO₂ lead to the production of sulfate and nitrate aerosols, and tropospheric
8 ozone (Seinfeld and Pandis, 1998). Volatile Organic Compounds (VOCs) oxidize in the presence
9 of NO_x and sunlight to form ozone (O₃), a major tropospheric pollutant and greenhouse gas
10 (EPA, 2013), and the oxidation product of NO₂, nitric acid (HNO₃), reacts with ammonia (NH₃)
11 to form ammonium nitrate aerosols. SO₂ is oxidized in gas-phase reactions with the hydroxyl
12 radical (OH) or in aqueous-phase reactions with O₃ or hydrogen peroxide (H₂O₂) to form sulfate
13 aerosols. Sulfate and nitrate aerosols contribute to fine particulate matter pollution with
14 aerodynamic diameters less than 2.5µm (PM_{2.5}). PM_{2.5} poses serious health concerns (Lee et al.,
15 2015; Liu et al., 2015), degrades visibility, causes acidification of water and the biosphere with
16 adverse effects on plants and soil, and impacts weather and climate through direct radiative
17 forcing and indirectly modifying cloud formation and optical properties (IPCC Working Group 1
18 et al., 2013; Twohy, 2005). SO₂, NO₂, and their oxidation products, O₃ and PM_{2.5}, are designated
19 Criteria Pollutants (European Commission, 2015; US EPA, 2016). Space-based characterization
20 of these pollutants enables global, consistent monitoring, which is independent from ground-
21 based measuring networks.

22 The first space-based quantitative data on SO₂ mass in volcanic clouds after a major eruption (El
23 Chichón,1982) was obtained from NASA's Nimbus-7 Total Ozone Mapping Spectrometer
24 (TOMS) (Krueger, 1983). The TOMS SO₂ detection sensitivity was limited by the instrument's
25 six narrow wavelength bands. In practice, only exceptionally strong anthropogenic SO₂ signals
26 could be detected, such as those produced by Norilsk smelting plants in Russia or from an
27 accidental combustion of elemental sulfur (S) at the Al-Mishraq State Sulfur Mine Plant in Iraq
28 (Carn et al., 2004; US Department of Veterans Affairs, 2015). Greatly improved sensitivity was
29 demonstrated through detection of SO₂ emissions from coal-fired power plants using ESA's
30 Global Ozone Monitoring Experiment (GOME, 1995-2005) (Burrows et al., 1997; Eisinger and
31 Burrows, 1998) and SCanning Imaging Absorption spectrometer for Atmospheric

1 CHartographY, (SCIAMACHY, 2002-2012) (Bovensmann et al., 1999) hyperspectral UV
2 spectrometers. The first tropospheric NO₂ quantification was demonstrated using GOME and
3 SCIAMACHY visible data (Leue et al., 2001; Martin et al., 2002; Richter and Burrows, 2002;
4 Richter et al., 2005). These sensors needed several days to acquire a contiguous global map. The
5 Ozone Monitoring Instrument (OMI) is the first satellite hyperspectral UV/Visible spectrometer
6 with a push broom CCD detector and a 2600 km wide swath (Levelt et al., 2006b), enabling
7 daily, global contiguous mapping of ozone and other trace gases, including SO₂ and NO₂ (Levelt
8 et al., 2006a). OMI was launched in July 2004 on NASA's Aura sun-synchronous afternoon
9 equator crossing polar satellite (Schoeberl et al., 2006) and continues measurements through its
10 12th year, providing the longest data record currently available.. NO₂ and SO₂ observations are
11 also made by two GOME-2 instruments on EUMETSAT's MetOp-A (2006) and B (2012)
12 operational polar satellites (Callies et al., 2000; Richter et al., 2011; Rix et al., 2012; Valks et al.,
13 2011) and Ozone Mapping and Profiler Suite (OMPS) on board the NOAA/NASA Suomi NPP
14 satellite (Dittman et al., 2002; Flynn et al., 2014; Seftor et al., 2014), which have coarser spatial
15 resolutions and higher detection thresholds for emissions from point sources (Fioletov et al.,
16 2013). ESA's next-generation Sentinel series will provide higher spatial resolution and greater
17 sensitivity to SO₂ and NO₂ sources (Ingmann et al., 2012; Veeffkind et al., 2012).

18 In the PBL, both SO₂ and NO₂ have short lifetimes (< 1 day during the warm season) and are
19 concentrated near their emission sources. This facilitates space-based detection of SO₂ and NO₂
20 sources and global characterization of their spatiotemporal variability (van der A et al., 2006,
21 2008; Burrows et al., 1999; Castellanos and Boersma, 2012; Eisinger and Burrows, 1998;
22 Fioletov et al., 2013; de Foy et al., 2009; Hayn et al., 2009; He et al., 2012; Hilboll et al., 2013;
23 Huang et al., 2013; Khokhar et al., 2005; Kim et al., 2009; Krotkov et al., 2008; Martin, 2008;
24 Martin et al., 2002; Mijling et al., 2009; Richter et al., 2005; Russell et al., 2012; Schneider and
25 Van Der A, 2012; Theys et al., 2015; Valks et al., 2011; Zhou et al., 2009, 2012) and near-
26 surface concentrations (Duncan et al., 2014; Lamsal et al., 2008, 2010, 2015; McLinden et al.,
27 2014, 2016). Furthermore, over polluted regions satellite observable SO₂ and NO₂ vertically
28 integrated number density profiles (columns) are highly correlated with underlying emissions,
29 allowing space-based (i.e., "top-down") inference of spatial and temporal changes in emissions
30 (van der A et al., 2008; Boersma et al., 2008, 2015; Carn et al., 2007; Ding et al., 2015; Duncan
31 et al., 2013; Fioletov et al., 2011, 2015; de Foy et al., 2014, 2015; Frost et al., 2006; Ghude et al.,

1 2010, 2013; Hayn et al., 2009; He et al., 2012; Kim et al., 2009; Konovalov et al., 2006, 2010;
2 Lamsal et al., 2011; Lee et al., 2011; Li et al., 2010; Lu et al., 2013, 2015; Martin, 2008;
3 McLinden et al., 2012, 2014; Miyazaki et al., 2012; Napelenok et al., 2008; Reuter et al., 2014;
4 Stavrakou et al., 2008; Streets et al., 2013; Vinken et al., 2014a, 2014b; Zhang et al., 2007),
5 lifetime (Beirle et al., 2011; Fioletov et al., 2011, 2015; de Foy et al., 2015; McLinden et al.,
6 2012), physicochemical conversion (Duncan et al., 2010; Valin et al., 2013) and deposition of
7 these species (Nowlan et al., 2014). OMI has been at the forefront of these rapid advances.

8 Previous OMI studies focused on specific species, emission sources and regions (van der A et al.,
9 2008; Ahmad et al., 2007; Beirle et al., 2011; Boersma et al., 2011, 2015; Castellanos et al.,
10 2014; Ding et al., 2015; Duncan et al., 2013; Fioletov et al., 2015, 2011; de Foy et al., 2009,
11 2015; Ghude et al., 2013; Lamsal et al., 2008, 2011, 2015; Lelieveld et al., 2015; Lu et al., 2013;
12 McLinden et al., 2014,2016; Mebust and Cohen, 2014; Mijling and Van Der A, 2012; Mijling et
13 al., 2009; Russell et al., 2012; Valin et al., 2013; Vinken et al., 2014a, 2014b; Zhou et al., 2012).
14 While NO₂ and SO₂ are both dominated by anthropogenic emissions in polluted regions, the
15 origin of their anthropogenic sources differs, as well as the cost and efficacy of their respective
16 emission control techniques. The often different regional trends and abundances of NO₂ and SO₂
17 offer valuable insights into energy infrastructures as well as pollution control policies (Li et al.,
18 2010; McLinden et al., 2014). In this paper we examine changes in both SO₂ and NO₂ over the
19 world's most polluted regions during the first decade of OMI observations. Section 2 briefly
20 summarizes OMI SO₂ and NO₂ algorithms and products. Section 3 describes regional SO₂ and
21 NO₂ changes for the world's industrial regions with large SO₂ emissions from coal burning
22 power plants and industries (Fig.1). For these regions we update the previously published OMI
23 trend studies (Duncan et al., 2013; Fioletov et al., 2011; Lu et al., 2013; Russell et al., 2012) and
24 provide a context for a more detailed analysis of individual sources (Duncan et al., 2016;
25 Fioletov et al., 2016; Lu et al., 2015). .

26 **2 OMI standard SO₂ and NO₂ products**

27 OMI is the result of a partnership between NASA and the Dutch and Finnish meteorological
28 institutes and space agencies (Levelt et al., 2006b) and flies on the NASA EOS-Aura satellite
29 (Schoeberl et al., 2006). It measures sunlight backscattered from the Earth over a wide range of

1 Ultraviolet (UV) and visible (Vis) wavelengths to derive abundances of ozone and other trace
2 gases important for air quality and climate. The measurements of SO₂ and NO₂ are both explicit
3 objectives of the Aura OMI mission (Levelt et al., 2006a) that are aimed at advancing our
4 understanding of the sources and transformation processes of these pollutants and enabling the
5 application of OMI data to inform public policy (Streets et al., 2013). Compared with other
6 satellite UV-Vis instruments, OMI has the highest spatial resolution, least degradation and the
7 longest record, allowing improved space-borne estimation of NO₂ and SO₂ emissions and the
8 study of their temporal behavior (Carn et al., 2007; Castellanos and Boersma, 2012; Duncan et
9 al., 2013; Fioletov et al., 2011, 2013; de Foy et al., 2009; Lamsal et al., 2015; Lu et al., 2013;
10 McLinden et al., 2012; Zhou et al., 2012).

11 Aura has a local equator crossing time of approximately 13:45 in the ascending node, and
12 provides nearly global coverage each day. The OMI detector is a 2-dimensional Charge-Coupled
13 Device (CCD) array. The instrument optics is designed such that the spatial dimension of the
14 detector is oriented across the orbit track, with an 115° field of view, while the other dimension
15 records spectral information. Three separate detectors (Dobber et al., 2006; Levelt et al., 2006b),
16 designated UV-1, UV-2, and Vis, have spectral coverage (full performance) in the ranges of
17 270–310 nm (spectral resolution, full width at half maximum (FWHM), of 0.63 nm), 310–365
18 nm (0.45 nm), and 365–500 nm (0.63 nm), respectively. The OMI SO₂ product uses spectral
19 measurements between 310.5 nm and 340 nm in the UV-2 (Li et al., 2013) and the NO₂ product
20 uses spectral measurements between 405 nm and 465 nm in the Vis region (Boersma et al., 2011;
21 Bucsela et al., 2013). The spatial dimension of both detectors is divided into 60 cross-track fields
22 of view (FOV) corresponding to the specific binned CCD detector rows, such that rows 1 and 60
23 correspond to the western and eastern edges of the swath, respectively. Spectral measurements
24 are made over 2-second exposure intervals. This results in along-track coverage of 13 km and
25 cross-track coverage of 24 km for the near-nadir FOVs (CCD rows about 30). During each orbit,
26 a total of about 1640 exposures are recorded on the sunlit side of the Earth. The width of the
27 swath (2600km) is such that 14-15 orbits per day are required to observe the entire surface of the
28 Earth, although with increased FOV size at the swath edges. Beginning in 2007, some cross-
29 track positions of the OMI swath were affected by FOV blockage and scattered light, also known
30 as the “row anomaly” (KNMI, 2012). Here we use only unaffected OMI cross track FOVs

1 throughout the entire mission, also excluding large FOVs at the edge of the swath, thus
2 considering only the values for CCD rows 6-23.

3 **2.1 Retrieval of PBL SO₂**

4 The original OMI PBL SO₂ product employed the band residual difference (BRD) algorithm,
5 which used only 4 discrete wavelengths (Krotkov et al., 2006). The BRD product is sensitive to
6 the large SO₂ point sources, but has a high noise level (Krotkov et al., 2008) and systematic
7 artifacts that required empirical corrections (Fioletov et al., 2011; Lee et al., 2009). In 2014, a
8 new PBL SO₂ product was released, in which SO₂ is retrieved with a new algorithm that employs
9 a principal component analysis (PCA) technique applied to OMI radiances (Li et al., 2013).
10 Using a clear sky Air Mass Factor (AMF) similar to the previous SO₂ product, but with the full
11 spectral content between 310.5 nm and 340 nm, the PCA algorithm reduces retrieval noise by a
12 factor of two (Li et al., 2013). Recently, the Differential Optical Absorption Spectroscopy
13 (DOAS) SO₂ algorithm developed for the Sentinel 5 Precursor (TROPOMI) has been applied to
14 the OMI radiances and compared with the operational PCA product (Theys et al., 2015). The two
15 products compare well, which lends confidence in OMI SO₂ data. The estimated SO₂ noise is
16 similar between PCA and DOAS algorithms, when using similar assumptions for AMF
17 calculation for pollution SO₂. However, the DOAS SO₂ algorithm requires empirical corrections
18 to remove background bias.

19 In this study we will use the OMI operational PCA PBL SO₂ product, which contains the
20 vertical column density (VCD) in Dobson Units (1 DU= 2.69×10^{16} molecules cm⁻²). The product
21 (OMSO2 v1.2.0) is publicly available from the NASA Goddard Earth Sciences (GES) Data and
22 Information Services Center (DISC) ([http://disc.sci.gsfc.nasa.gov/Aura/data-](http://disc.sci.gsfc.nasa.gov/Aura/data-holdings/OMI/omso2_v003.shtml)
23 [holdings/OMI/omso2_v003.shtml](http://disc.sci.gsfc.nasa.gov/Aura/data-holdings/OMI/omso2_v003.shtml)). For background areas the estimated 1σ noise is ~ 0.5 DU (1
24 $\text{DU} = 2.69 \times 10^{16}$ molecules cm⁻²) over tropical oceanic areas (Li et al., 2013). If we assume that
25 the noise is random and that there are about 100 cloud-free samples per year, the detection limit
26 over low latitudes is estimated to be 4 times the mean error: ~ 0.2 DU for the annual mean. For a
27 single retrieval over polluted areas, random error due to instrument noise is typically on the order
28 of 50-100%. The systematic uncertainties due to our use of fixed Jacobians are 50-100% for
29 cloud-free scenes. The total error for a single retrieval is 70-150%. For an annual average the
30 uncertainties due to the retrieval noise are reduced to the level of 10-15% of the actual signal,

1 and become insignificant relative to the systematic errors. The systematic errors could be further
2 reduced to the level of 20% applying improved local Jacobians (McLinden et al., 2014, 2016).
3 An important advantage of the PCA algorithm is that the bias over background regions (where
4 SO₂ columns are below the OMI detection limit) is sufficiently small (< 0.1 DU) that it requires
5 no empirical background correction, as applied in other satellite SO₂ algorithms (e.g., Fioletov et
6 al., 2013; Theys et al., 2015). The improved data quality, combined with the pixel averaging and
7 oversampling techniques (e.g., de Foy et al., 2009; Fioletov et al., 2011, 2013, 2015; Lu et al.,
8 2013; McLinden et al., 2014,2016), provides greatly enhanced sensitivity to anthropogenic SO₂
9 sources near the surface (Fioletov et al., 2016; McLinden et al., 2014). It has been demonstrated
10 that US SO₂ point sources (e.g., power plants, smelters) with emissions rates as low as ~30-40
11 kt y⁻¹ can be detected and analyzed using the PCA OMI SO₂ product (Fioletov et al., 2015). This
12 limit is substantially lower than that reported (70 kt y⁻¹) for the previous version OMI SO₂ data
13 (Fioletov et al., 2011).

14 **2.2 Retrieval of tropospheric NO₂**

15 There are two algorithms used operationally to determine tropospheric NO₂ VCDs: the NASA
16 standard product (SP, version 2.1) and the KNMI Dutch-OMI-NO₂ (DOMINO) algorithm
17 (TM4NO2A, version 2, <http://www.temis.nl/airpollution/no2.html>) (Boersma et al., 2011). Both
18 products share a common DOAS spectral fitting of the OMI-measured, sun-normalized
19 backscattered radiances to laboratory-measured absorption spectra of NO₂, H₂O, and O₃, and a
20 calculated Ring pseudo absorption spectrum (Chance and Spurr, 1997), to give NO₂ slant column
21 densities (SCDs). The estimated 1σ noise is ~10¹⁵ molecules cm⁻² or ~10% of the measured SCD
22 over polluted regions (Boersma et al., 2011). The SCDs, after subtraction of the stratospheric
23 contribution are converted to tropospheric VCDs by applying AMFs interpolated from the Look-
24 up-Tables (LUT) with OMI-measured input parameters such as viewing geometry,
25 climatological surface reflectivity, cloud pressure and cloud radiance fraction, assuming *a priori*
26 NO₂ vertical profile shapes. The NASA and KNMI algorithms differ in how they remove the
27 stratospheric contribution and use different *a priori* tropospheric NO₂ profile shapes in the AMF
28 calculation. DOMINO subtracts stratospheric SCD as determined in a data assimilation system,
29 in which the measured SCDs are assimilated with the TM4 chemical transport model (Boersma
30 et al., 2011). The SP estimates stratospheric NO₂ from OMI data without using stratospheric
31 chemical transport models directly. The AMFs are calculated with *a priori* NO₂ monthly mean

1 vertical profile shapes from the NASA GMI model (Bucsela et al., 2013). Despite the
2 differences, both algorithms produce statistically similar regional trends (see Supplementary
3 Material Fig. S1). Here we use the SP tropospheric NO₂ VCD product version 2.1 publicly
4 available from NASA GES DISC at [http://disc.sci.gsfc.nasa.gov/Aura/data-](http://disc.sci.gsfc.nasa.gov/Aura/data-holdings/OMI/omno2_v003.shtml)
5 [holdings/OMI/omno2_v003.shtml](http://disc.sci.gsfc.nasa.gov/Aura/data-holdings/OMI/omno2_v003.shtml). Over polluted areas the total errors in OMI tropospheric NO₂
6 VCDs are typically less than 20% for cloud-free FOVs, as confirmed by validation studies
7 employing *in-situ* and remotely sensed data (Bucsela et al., 2013; Irie et al., 2012; Lamsal et al.,
8 2015; Oetjen et al., 2013).

9 **2.3 Postprocessing of NO₂ and SO₂ data**

10 For this study, level 2 (L2) tropospheric NO₂ and PBL SO₂ VCDs are gridded at different ground
11 resolutions after excluding FOVs possibly affected by the 1) row anomaly; 2) snow; 3) transient
12 volcanic SO₂ clouds (Appendix A); 4) cloudy scenes with cloud radiance fraction, CRF > 0.5 for
13 NO₂ or CRF > 0.2 for SO₂. We note that the CRF is approximately twice as large as the
14 effective cloud fraction derived assuming Mixed Lambert-Equivalent Reflectivity (MLER) cloud
15 model (Boersma et al., 2011; Bucsela et al., 2013; Stammes et al., 2008). Given the very small
16 CRF thresholds, the remaining cloud related errors were estimated to be less than 20% (Lee et
17 al., 2009; McLinden et al., 2014). However, by selecting mostly clear sky conditions, our
18 sampling of the OMI dataset may introduce a bias relative to all-sky conditions (Geddes et al.,
19 2012; McLinden et al., 2014). Clouds are also associated with certain weather conditions, which
20 in turn may affect the level of pollution. These factors may introduce biases in our derived trends
21 in SO₂ and/or NO₂, but only if there is significant, long-term shift in weather regimes. However,
22 for polluted regions in Fig.1 satellite derived regional trends in cloud reflectivity (less than +/-
23 2% per decade (Herman et al., 2013)) are much smaller than those caused by changes in
24 emissions (see section 3).

25 The standard gridded (0.25° × 0.25°) level 3 (L3), filtered, monthly regional mean values
26 are used in time series analyses following Lamsal et al. (2015) (Appendix B). The L3 data are
27 publicly available from NASA GES DISC archive at [http://disc.sci.gsfc.nasa.gov/Aura/data-](http://disc.sci.gsfc.nasa.gov/Aura/data-holdings/OMI)
28 [holdings/OMI](http://disc.sci.gsfc.nasa.gov/Aura/data-holdings/OMI). We also use L2 (pixel level) data oversampled at higher resolutions (0.01° ×
29 0.01° for NO₂ and 0.02° × 0.02° for SO₂) to create global and regional maps that highlight point
30 pollution sources. The regional maps are created directly from pre-filtered L2 data by averaging

1 all OMI pixels within 20 km smoothing radius (30 km for SO₂) for 3 year time periods. Unlike
2 previous studies (Lee et al., 2009; Fioletov et al., 2011, 2013; Lu et al., 2013; McLinden et al.,
3 2014), no empirical background correction was applied to the PBL SO₂ data.

4 **3 Regional pollution changes and interpretation**

5 Figure 1 shows SO₂ and NO₂ multi-year average maps at the beginning of the OMI mission
6 (2005-2007) over the northern hemisphere. Regionally, population density (Lamsal et al., 2013),
7 type of power generation and fuel used, economic activity, and regulatory policies determine
8 average levels of air pollution. The SO₂ map (Fig. 1a) shows hotspots associated with major
9 coal-fired power plants and industrial activities, such as oil and gas refining and metal smelting.
10 The highest SO₂ is found over industrialized and populated regions in eastern China, as the
11 world's second-largest economy relies on sulfur (S)-rich coal for ~70% of its energy
12 consumption (Klimont et al., 2009; Zhang and Cheng, 2009; Wang et al., 2015). Based on
13 bottom-up emission inventories, SO₂ emissions from China were the world's largest, at ~33 Tg
14 SO₂ in 2005 (Lu et al., 2010, 2011). High S coal-fired power plants are the major contributors to
15 the SO₂ over the eastern US (SO₂ emissions 14.5 Tg SO₂ in 2005 (US EPA, 2015)), eastern
16 Europe and India (~6.7 Tg SO₂ (Lu et al., 2011)). SO₂ is undetectable over the western US and
17 western Europe, where emissions of SO₂ have been relatively small due to a smaller proportion
18 of coal-fired power plants, the low S content of coal, and installation of effective flue gas
19 desulfurization devices (FDG) capable of capturing more than 95% of SO₂ emissions (US EIA,
20 2010).

21 Large SO₂ column amounts are also observed over the Persian Gulf, due to emissions
22 from the oil and gas industry, gas flaring and shipping in the region. Based on a bottom-up SO₂
23 emission inventory, the total SO₂ emissions from the Middle East in 2005 were ~6 Tg SO₂
24 (Smith et al., 2011), less than those from India and the US. However, OMI-observed SO₂
25 columns over the Persian Gulf region are significantly larger than over these two regions. This
26 implies that real SO₂ emissions from the Middle East (particularly in the Persian Gulf) are
27 significantly underestimated in current bottom-up emission estimates.

28 In addition to anthropogenic SO₂, volcanic SO₂ is frequently observed over Kamchatka
29 (Russian Federation), Japan, the South Pacific (e.g., Anatahan volcano, Mariana Islands, Mauna

1 Loa, Hawaii), Sicily (Etna), Mexico (Popocatepetel volcano, south of Mexico city), Central
2 America and Montserrat, West Indies. Although transient volcanic signals were filtered from the
3 PBL SO₂ data (Table A1), the signals from frequently erupting (e.g., Mt. Etna, Popocatepetel) or
4 degassing volcanos remain. Except for Mt. Etna, Iceland volcanoes (Ialongo et al., 2015;
5 Schmidt et al., 2015), and Mt. Popocatepetel (de Foy et al., 2009), most volcanic sources are
6 located in remote locations and do not contribute to the SO₂ in industrial regions considered here
7 (see OMI daily SO₂ maps for the world's volcanic regions at <http://so2.gsfc.nasa.gov>).

8 The average OMI NO₂ map (Fig.1b) is correlated with the nighttime lights map (Fig.1c),
9 used here as a proxy for population density and energy production (Lamsal et al., 2013). For
10 example, the highest NO₂ levels are observed over the world's most populated and industrialized
11 regions, including eastern China, western Europe, and the eastern US, where local NO₂ "hot
12 spots" coincide with large urban agglomerations (Schneider et al., 2015), power plants (Duncan
13 et al., 2013; de Foy et al., 2015), and industrial complexes. NO₂ tropospheric columns over India
14 and the Middle East are significantly less than those over China, western Europe and the US.
15 This can be explained by low NO_x emissions, especially from mobile sources, and, partly, by
16 year-round high temperatures, leading to shorter NO₂ lifetimes (Beirle et al., 2011). For example,
17 Indian NO_x emissions were relatively low, at 5.7 Tg NO_x in 2005 (Lu and Streets, 2012),
18 whereas those from China and the US were 16.9 Tg NO_x (Klimont et al., 2009) and 20.4 Tg NO_x
19 (US EPA, 2015), respectively. Relatively small, but significant, areal NO₂ enhancements over
20 west African forest are caused by seasonal biomass burning NO_x emissions (Mebust and Cohen,
21 2014).

22 The differences between the spatial distributions of NO₂ and SO₂ over the large regions
23 indicated as boxes in Fig. 1a and 1b are related to economic activity, fuel types, combustion
24 technology and different regulatory policies. The most abundant source of SO₂ is Pyrite (FeS₂)
25 and organic S in lower-grade coal as well as liquid fuel, mostly contained in heterocyclic
26 aromatic compounds in oil, which largely accounts for high SO₂ levels over the Persian Gulf
27 from gas flaring and oil refining. Many developed countries have regulated the S content of fuels
28 and also required catalytic exhaust gas processing, resulting in decreased mobile-source NO_x and
29 SO₂ emissions in exhaust. Regulations are also focused on stack emissions of NO_x and SO_x (SO_x
30 = SO₂ + SO₃) at point sources, such as power plants and smelters. This, in turn, has driven

1 technological changes upstream to meet regulatory requirements. For example, fluidized-bed
2 combustion technology permits burning at lower temperature, producing less NO_x, and
3 condensed phase chemical capture of S, producing less gaseous SO_x. Chemical Loop
4 Combustion technology uses catalytic oxygenation to oxidize the fuel largely in the absence of
5 N₂, again resulting in greatly reduced NO_x leaving the combustion chamber. Stack scrubbers
6 (i.e., flue gas desulfurization devices, FDG) have been widely deployed in Europe and the US, in
7 particular, for existing plants, to remove SO₂ and other chemicals—notably mercury—from the
8 flue gases, in order to meet regulatory standards. However, these changes have yet to be widely
9 implemented in developing countries.

10 In addition to emissions, meteorology also plays an important role in regional air
11 pollution, particularly on relatively short time scales (days to months). For midlatitude areas
12 discussed in this study (the eastern US, eastern China, and eastern Europe), the concentrations of
13 SO₂ and NO₂ often exhibit large day-to-day changes. They tend to increase under the relatively
14 stagnant conditions ahead of a cold front and decrease dramatically after the cold front brings
15 precipitation and strong winds into the area (Li et al., 2007). On the interannual time scale, the
16 frequency of cold front passages may be influenced by large-scale circulation patterns such as
17 the position of the Siberian high for eastern China (Jia et al., 2015), leading to interannual
18 changes in SO₂ and NO₂. But meteorology probably plays a lesser role in the longer-term trends
19 that we discuss in this study. For example, given the general trend of weakening surface winds in
20 the northern hemisphere (Vautard et al., 2010), one would expect both SO₂ and NO₂ to increase
21 over time in China, with constant emissions. While OMI did initially observe growths in both
22 SO₂ and NO₂ over China (section 3.3), the different trends between the two gases after 2007
23 imply that different emission control measures may play a more significant role in OMI-
24 observed trends. Similarly, the decreasing pollution levels observed over the eastern US (section
25 3.1) and eastern Europe (section 3.2) can only be explained by a reduction in emissions. As for
26 tropical areas such as India, the impact of year-to-year fluctuations in OMI SO₂ and NO₂ data
27 caused by meteorological variations is small relative to the observed fast growth in emissions
28 that occurred over areas with newly built power plants and many cities (section 3.4).

29 Another factor that can potentially affect derived long-term trends is long-term changes
30 in the vertical profile shape, because our a priori profiles are constant for the entire mission. We

1 believe that the impacts are relatively minor for OMI measurements, as the boundary layer is
2 often thick and quite well mixed during OMI overpass time (in local afternoon). Our previous
3 aircraft measurements over northeastern China and the eastern US show that the difference in
4 AMF due to different SO₂ profile shapes over the two regions are very small (within a few
5 percent, see Krotkov et al. 2008 for more detailed discussion).

6 With this understanding of the influence of different factors on anthropogenic NO₂ and
7 SO₂ columns, we turn, in the remainder of this section, to examining regional decadal trends as
8 seen by OMI measurements. We examine five regions indicated in Fig.1: the eastern US, eastern
9 Europe and Turkey, eastern China, India, and the Middle East, which all have SO₂ and NO₂
10 sources detectable by OMI. The regions are in different phases of economic development and
11 environmental regulations. We can therefore compare and contrast the trends in SO₂ and NO₂
12 that have different sources depending on the types of fuels burned, industrial activity, and
13 regulations.

14 **3.1 Eastern US**

15 Over the eastern US the highest levels of SO₂ were observed in areas of intense high-S coal
16 combustion for industrial processes and electricity generation, including the Ohio River Valley
17 and SW Pennsylvania (ORV, blue box in Fig. 2). Concentrations are undetectable over the
18 western US where the local coal is intrinsically lower in S and emissions of SO₂ have been
19 relatively small (US EIA, 2010). Prior investigations involving OMI have reported a 40% SO₂
20 reduction near power plants in the eastern US between 2005 and 2010 (Fioletov et al., 2011).
21 More recent OMI observations (Fig. 2) show that the SO₂ levels continued to drop after 2010 due
22 to both national (e.g., Clean Air Interstate Rule, CAIR (CAIR, 2009)) and state regulations, such
23 as 2005 Maryland Healthy Air Act (HAA) (He et al., 2016). Currently, US regional SO₂ levels
24 are at or below the OMI SO₂ detection limit of ~0.2 DU. The dramatic decrease over the course
25 of the first 11 years of the OMI mission (Fig. 2) closely matches trends in reported SO₂
26 emissions (US EPA, 2015) and sulfate deposition (-5%/yr decrease over the eastern US from
27 2000-2010 (Hand et al., 2012; Solomon et al., 2014)) and has also been observed from surface
28 and aircraft measurements (He et al., 2016). This striking improvement in SO₂ coincides with
29 implementation of control technology, such as flue gas desulfurization (FGD), closure of some
30 of the oldest coal power plants and fuel switching from coal to natural gas. Reductions in SO₂

1 emissions are required by the 1990 Clean Air Act Amendments (CAAA, 1990) and other
2 regulations. Substantial success has been achieved through market-based cap and trade programs
3 such as the Acid Rain Program (ARP, 2010) and The Clean Air Interstate Rule (CAIR, 2009).
4 These allow electricity producers to pick the most economical emission control methods. The
5 conversion to natural gas with much less fuel S than coal has also contributed to the reduction in
6 SO₂ pollution.

7 Unlike SO₂, which originates primarily from fuel-bound S, all high-temperature
8 combustion, including internal combustion engines, can generate NO_x. As expected, OMI NO₂
9 columns peak over major cities and highways, as well as over clusters of power plants. Chicago,
10 Atlanta, and the megalopolis from Washington, DC to New York, also called the I-95 corridor
11 (red box in Fig.2), stand out. At the beginning of the OMI mission in 2005, a broad background
12 of elevated NO₂ was detected over rural areas of the eastern US underlying the hot spots over
13 large metropolitan areas (Fig. 2). Since that time, NO₂ has significantly decreased as a result of
14 emission regulations on power plants and cars (Duncan et al., 2013; Lamsal et al., 2015; Lu et
15 al., 2015; Russell et al., 2012). Decreases in NO₂ are evident in OMI NO₂ data over all major
16 cities (Lu et al., 2015; Tong et al., 2015), especially over the I-95 corridor (red box in Fig. 2 and
17 Fig. S1). NO₂ from clusters of power plants has also decreased (e.g., ORV, blue box in Fig. 2). In
18 general, downward trends in OMI NO₂ data near US power plants correlate well with trends in
19 NO_x emissions from the Continuous Emissions Monitoring System (CEMS) (Duncan et al.,
20 2013) and with surface NO₂ concentrations reported by EPA Air Quality Systems (AQS)
21 (Lamsal et al., 2015; Lu et al., 2015; Tong et al., 2015). The NO₂ reductions are due to selective
22 catalytic reduction (SCR) on point sources and three-way catalytic converters on vehicles
23 (Russell et al., 2012).

24 Figure 3 (upper row) compares year-to-year changes in the OMI SO₂ and NO₂ annual
25 columns and bottom-up emissions from power plants over the ORV region (blue box in Fig. 2)
26 with other heavily polluted regions discussed later. Overall, between 2005 and 2015 the SO₂
27 drop over ORV was close to 80%, while NO₂ dropped by 40%, the largest reductions seen in this
28 study. Previous studies demonstrate a linear ~1:1 relationship between the percent change in NO_x
29 or SO₂ emissions from isolated power plants and the corresponding changes in OMI columns
30 (Fioletov et al., 2011, 2015; de Foy et al., 2015). However, Duncan et al. (2013) show that most

1 power plants, such as in the eastern US, are co-located with mobile NO_x sources, so that this
2 relationship is not always obvious. Indeed, OMI observed smaller drop in NO₂ columns (~40%)
3 than would have been expected from ~60% reduction in NO_x emissions from the power plants in
4 the region (Fig. 3).

5 The magnitude of the relative reduction in NO₂ over the I-95 corridor is similar to that
6 over the ORV (SM: Fig. S1), suggesting similar reduction in NO_x emissions from cities and
7 mobile sources. Independent analysis of OMI NO₂ data confirmed that NO_x emissions of 35
8 major US urban areas decreased by ~50% from 2006 to 2013 (Lu et al., 2015). We also note the
9 faster decline in NO₂ levels before 2009 because of the installation of NO_x emission control
10 devices (ECDs) on power plants and impact of the economic recession in 2007-2009. Power
11 plants that were already operating ECDs during the ozone season began operating them year-
12 round (Lamsal et al., 2015). The annual reduction rate in NO₂ has slowed since 2009 as the US
13 economy has recovered from the recession and the implementation of further pollution controls
14 has slowed.

15 Although both SO₂ and NO₂ are Criteria Pollutants, and there remain jurisdictions in the
16 US in violation of the National Ambient Air Quality Standards (NAAQS) for these primary
17 pollutants, just as important is their role as precursors of key secondary air pollutants such as fine
18 particles (PM_{2.5}) and ozone. The greatest numbers of Americans at risk for harmful effects of air
19 pollution are subject to exposure to these secondary pollutants (Lee et al., 2015). By 2015, total
20 US SO₂ emissions fell to about 1/6 of their 1970 peak, but NO_x emissions only fell substantially
21 after 2000 and are now about ½ of their peak in 2000 (<http://www.epa.gov/ttnchie1/trends/>).
22 Because of these NO_x reductions, photochemical smog over eastern US has improved
23 significantly over the same time period (Castellanos et al., 2011; Hogrefe et al., 2011; Simon et
24 al., 2015). The total deposition of oxidized N (the combination of wet and dry deposition of
25 species such as NO₂ and NO₃⁻) has improved as well (Nowlan et al., 2014) indicating that the
26 efforts to control NO_x emissions have been successful. As result of larger SO₂ reductions, the
27 SO₂/NO₂ column ratio dropped over the ORV region from its maximal values of ~4-5 in 2005 to
28 less than 2 in 2012 (SM, Fig. S2). We expect similar change in PM speciation with increasing
29 relative contribution of nitrate aerosols.

30

1 **3.2 Eastern Europe**

2 Europe experienced a ~80% reduction in SO₂ emissions between 1990 and 2011 (EEA, 2013).
3 Particularly, in western Europe, after significant reduction of SO₂ emissions in the 1980s-1990s,
4 the SO₂ levels have dropped below the OMI detection limit of ~0.2 DU. There are, however,
5 detectable SO₂ sources in eastern Europe (Fig. 4). The spatial distribution of the observed SO₂
6 columns at the beginning of OMI mission is consistent with the spatial pattern of SO₂
7 concentrations derived from the surface monitoring stations for 2005 (Denby et al., 2010).
8 Notable anthropogenic SO₂ sources include, for example, the mining and industrial districts in
9 Donbass region in Eastern Ukraine, large coal-fired thermal power plants around the Sea of
10 Marmara and those near Kahramanmaras in southern Turkey, as well as those near Galabovo in
11 Bulgaria, Gorj County in southwestern Romania, Belgrade in Serbia, and Megalopoli in southern
12 Greece (Fioletov et al., 2016). Most of SO₂ hot spots are due to use of local high S lignite
13 (brown) coal for power generation and incomplete SO₂ removal from the flue gas. Fig. 3 (second
14 row) shows interannual variations in SO₂ and NO₂ columns over the Maritsa Iztok power
15 complex in Stara Zagora, Bulgaria (see blue box in Fig. 4). Large SO₂ reductions (~50%)
16 between 2011 and 2015 are consistent with the installation of FGD, while NO₂ remains
17 approximately constant, suggesting stable electricity production. Another important source of
18 SO₂ in the region is the Mt. Etna volcano, in Sicily. OMI SO₂ retrievals indicate considerable
19 decreases in SO₂ over Megalopoli, Galabovo, and Gorj County, likely owing to more stringent
20 SO₂ controlling measures on power plant emissions in response to mandates by the European
21 Union. SO₂ emissions from Turkey, on the other hand, have increased during the same period,
22 particularly over Kahramanmaras, where new power plants went into service in 2006 (see
23 <http://globalenergyobservatory.org/geoid/42972>). Increases in SO₂ over Serbia may reflect
24 growth in energy consumption (mainly from coal) as the country's economy recovers from wars
25 in the 1990s.

26 Figure 4 (bottom row) gives the spatial distribution of OMI tropospheric NO₂ over
27 eastern Europe, which shows enhanced columns in densely populated and industrial areas. By far
28 the largest NO₂ was observed over Moscow, Russian Federation, confirmed by in situ
29 measurements at different heights within PBL (Chubarova et al., 2009, 2016; Elansky et al.,
30 2007; Gorchakov, 2011). In Moscow maximal surface concentrations exceed 100 ppb for NO₂,
31 but are less than 2 ppb for SO₂ (Elansky et al., 2007). OMI also observed large NO₂ over

1 industrial regions near Katowice in south Poland, east Germany and the northwestern Czech
2 Republic. Elevated NO₂ columns are evident over large cities, such as Istanbul, Prague, Warsaw,
3 Vienna, Rome, Athens, and Budapest. These enhancements correlate well with emissions source
4 distribution (Janssens-Maenhout et al., 2015). While road traffic is in general the most important
5 NO_x source in Europe (EEA, 2013; Vestreng et al., 2009), in some eastern European countries
6 the power sector is the major contributor (Zyrichidou et al., 2013). New construction and
7 upgrades in capacity of older power plants, as well as emission control measures affect NO₂
8 columns (Castellanos and Boersma, 2012; Zhou et al., 2012). Several studies based on bottom-up
9 emissions and satellite observations have reported substantial decreases in NO_x emissions and
10 NO₂ columns in most of the western European countries due to stricter emission regulations
11 (Castellanos and Boersma, 2012; Curier et al., 2014; EEA, 2013; Lamsal et al., 2011; Schneider
12 et al., 2015; Vestreng et al., 2009; Zhou et al., 2012). In contrast, changes in emissions are rather
13 small in eastern Europe (Zyrichidou et al., 2013). An increase in NO_x emissions is reported for
14 those countries where implementation of the European Union (EU) air quality standards is less
15 effective (AQ_Environment_EC, 2015; Vestreng et al., 2009). OMI measurements are consistent
16 with previous studies, suggesting small or insignificant NO₂ column trends on a regional level.
17 Changes appear to be country-specific and likely depend on the socio-economic and political
18 situation and legislative abatement measures of the country. The EU air quality standards hold
19 for all EU-countries (including Poland, Hungary, Bulgaria, Croatia, the Baltic States, Slovenia,
20 Slovakia), but not for Serbia, Russia, Ukraine, Belarus, and Turkey. Some countries have asked
21 for a time extension to meet certain standards because several member States have particular
22 difficulties in achieving compliance with the criteria for PM and NO₂.

23 **3.3 Eastern China**

24 The growth of the Chinese economy over the past two decades has been mainly driven by rapid
25 industrialization and urbanization (Huang et al., 2013) and has been accompanied by large
26 increases in both electricity generation (mainly coal-fired power plants) and the number of
27 vehicles on Chinese roads. As evident in Fig. 1a and 5, China has the world's highest SO₂
28 emissions, particularly over the high S coal-rich, heavily industrial areas in Hebei, Henan, and
29 Shandong provinces in the North China Plain (NCP, blue box in Fig. 5), Inner Mongolia (Li et
30 al., 2010; Zhang et al., 2009), the highly populated Sichuan Basin (SB, red box in Fig.5), the
31 megacity clusters around Shanghai (the Yangtze River Delta, YRD – black box in Fig. 5) and

1 Guangzhou-Hong Kong (the Pearl River Delta, PRD). Similarly, OMI retrievals also reveal
2 much greater NO₂ over eastern China than other regions of the world (Fig. 1b), especially over
3 NCP, YRD and PRD (Fig. 5). The NO₂ levels are relatively low over SB, but higher over YRD
4 and PRD. The SO₂/NO₂ column ratios were 8-10 over SB, 3-5 over NCP and less than 2 over
5 YRD and PRD in 2005 (Fig. S4). The ratios reflect to some extent the level of modernization in
6 the regions. The PRD and YRD have relatively less coal-fired power plants but higher
7 population and car density, therefore greater NO₂ relative to SO₂.

8 The overall SO₂ loading, although still at a relatively high level, has decreased over the
9 recent years (Fig. 5). This is more clearly shown in the SO₂ time series in Fig. 3, which suggests
10 that the SO₂ loading over the NCP peaked in 2007, and has since shown an overall decreasing
11 trend despite relatively large year-to-year variations. The reduction in SO₂ during 2008-2010
12 may be attributed to both the economic recession and emission control measures before the 2008
13 Beijing Olympic Games (Li et al., 2010; Lu et al., 2011; Mijling et al., 2009; Witte et al., 2009).
14 The temporary rebound in 2011 may reflect a resurgence in the economy due to stimulation by
15 the government. This is followed by a dramatic ~60% reduction over the four-year period during
16 2012-2015, which may be attributed to both stricter emission reduction targets during the 12th
17 Five-Year Plan (2010-2015) (Tian et al., 2013; Zhao et al., 2013), more widespread use of FGD
18 on coal-fired power plants and industries (Wang et al., 2015), as well as a slowdown in the
19 growth rate of the Chinese economy. We confirmed the 2012-2015 SO₂ reduction over NCP
20 applying our SO₂ retrievals to the measurements from the Ozone Mapping and Profiler Suite
21 (OMPS) instrument on board NASA-NOAA Suomi National Polar Partnership (SNPP) satellite
22 (Fig. S3). In relative terms the SO₂ reduction in 2005-2015 was larger over YRD and SB regions
23 compared to NCP (Fig. S3).

24 NO₂ over NCP, on the other hand, peaked in 2011 after dramatic ~50% increase since
25 2009 (Fig. 3) and decreased slightly in 2012 and 2013 (Fig. 3). Temporary drop in 2008 can be
26 attributed to strict pollution reduction measures implemented before 2008 Olympic games and
27 economic recession. The reductions were strongest in Beijing, Tianjin and Schijiazhuang regions
28 (Mijling et al., 2009; Witte et al., 2009). The dramatic ~40% drop in NO₂ in 2014-2015 is likely
29 a result of the slowest economic growth rate for China in nearly 25 years. According to the
30 National Bureau of Statistics, the electricity generation by thermal power plants decreased by

1 several percent in the second half of the year as compared with 2013. Similarly there is also a
2 slowdown in coal-intensive industrial sectors (Guay, 2015) and stricter emission control policies
3 (MEP, 2013). Independent satellite NO₂ retrievals with GOME-2A, GOME-2B and OMI also
4 confirm large reduction in NO₂ over eastern China between 2013 and 2014 (Richter et al., 2015).
5 Over SB and YRD NO₂ columns peaked in 2010 and remained relatively constant afterwards
6 (Fig. S1). As a result of the different trends between SO₂ and NO₂ the SO₂ to NO₂ ratios dropped
7 to their lowest values of ~2-3, ~1-2 and less than one over SB, NCP and YRD regions,
8 respectively (Fig. S4).

9

10 **3.4 India**

11 Figure 6 shows multi-year mean OMI SO₂ and NO₂ maps over India. A number of SO₂ and NO₂
12 hot spots are observed, and they match the locations of large coal-fired power plants and major
13 cities (Ghude et al., 2011, 2013). This is because coal-fired power plants are the dominant SO₂
14 and NO_x emission sources in India, and they are often built near large cities where other
15 anthropogenic emissions are also high. Fig. 6 also shows that from 2005 to 2015, there was an
16 increase in the OMI-observed SO₂ and NO₂ columns over India, mainly reflecting the fast
17 expansion of the power sector driven by rapid economic growth. Based on an updated unit-based
18 coal-fired power sector database (Lu and Streets, 2012; Lu et al., 2013), the total installed
19 capacity, power generation, and fuel consumption of Indian coal-fired power plants increased
20 dramatically by 126%, 91%, and 93%, respectively, during 2005-2014. The SO₂ emissions from
21 power plants are high, because S in local coal is mostly in organic form and cannot be removed
22 by physical cleaning methods (Lookman and Rubin, 1998).

23 Unlike the US, Europe, and China, SO₂ and NO_x emitted from coal-fired power plants are
24 not regulated in India and the installation and operation rates of SO₂ and NO_x emission control
25 devices are very low. FGD devices for SO₂ were reported to be operating in only three power
26 plants at the beginning of OMI mission (Chikkatur et al., 2007). NO_x emissions by coal-fired
27 power plants are also not regulated in India. Although some new plants were reported to be
28 equipped with low-NO_x burners (LNB), the actual installation rate and performance of these
29 LNB devices are not known. Based on bottom-up emission inventories we estimate that SO₂ and

1 NO_x emissions from Indian coal-fired power plants increased by 103% and 94%, respectively,
2 during 2005-2014 (Lu and Streets, 2012; Lu et al., 2013).

3 As shown in Fig.3, the growth rates in OMI-observed SO₂ (200%±50%) and NO₂
4 (50%±20%) columns during 2005-2015 were particularly large over the industrial regions in
5 Chhattisgarh and Odisha (blue box in Fig. 6), one of India's most active areas in terms of
6 building new power plants. By the end of 2014, the total installed capacity of coal-fired power
7 plants in this region was 28 GW, 85% of which (~24 GW) was installed after 2005, accounting
8 for ~26% of the total newly installed capacity in India. As a result, SO₂ and NO_x emissions from
9 coal-fired power plants in this region were estimated to increase both by ~190% from 2005 to
10 2014 (Lu and Streets, 2012; Lu et al., 2013), largely in line with OMI SO₂ observations (Fig.3g).
11 India's total annual SO₂ emissions almost doubled from 6.7 Tg in 2005 to estimated 12 Tg in
12 2014. In 2014, India has not only surpassed the US to be the world's second largest SO₂ emitting
13 country, but also has reached more than 40% of the SO₂ emissions of the world's largest emitter,
14 China.

15 During the last decade OMI observed much smaller NO₂ increases (~50%) than one
16 would have expected from the increase in NO_x emissions from the coal-fired power plants (Fig.
17 3h). One possible explanation for the discrepancy might be relatively high NO₂ background from
18 other emission sources. While coal-fired power plants may be the single largest contributor to
19 SO₂ in this region, transportation is a larger contributor to NO_x, and the slower increase in
20 transportation emissions could have masked the sharp increase in coal-fired power plants NO_x
21 emissions. In India, the prevalence of motorcycles with small, two-stroke engines lead to high
22 transportation emission factors for CO, VOC and PM, but produce only modest amounts of NO_x
23 (Dickerson, 2002). Also, with a 3-fold increase in NO_x emissions from the power plants, there
24 could be some non-linear effects in NO_x chemistry, changing the lifetime of NO₂. Heavy
25 loadings of soot may also remove NO₂ (Dickerson, 2002). The discrepancies will be addressed in
26 future studies.

27

1 **3.5 Middle East**

2 In the Middle East, abundant oil and gas deposits supply cheap and relatively clean fuels for
3 electricity generation, water desalination, and industries. OMI detects the largest SO₂ emissions
4 over the Persian Gulf. The sources for these emissions are apparently not included in the current
5 global emission inventory such as EDGAR-HTAP dataset (Janssens-Maenhout et al., 2015).
6 Based on the most recent SO₂ emission inventory, the total SO₂ emissions from the Middle East
7 in 2005 were ~6 Tg (Klimont et al., 2013; Smith et al., 2011), less than those from India and the
8 US. However, OMI observed SO₂ columns over the Gulf region are significantly larger than
9 those over India and US. That suggests that the real SO₂ emissions from the Middle East
10 (particularly in the Persian Gulf) may be several times higher than current bottom-up emission
11 estimates. This is consistent with independent OMI SO₂ retrievals (Theys et al., 2015). Inverse
12 modeling using OMI and SCIAMACHY retrievals also suggests an underestimate of SO₂
13 emissions from the Persian Gulf (Lee et al., 2011).

14 In-situ measurements of SO₂ and other pollutants are rarely reported for the region, but
15 available data generally indicate significant SO₂ loading over the Persian Gulf. For example, an
16 aircraft campaign conducted north of the United Arab Emirates during winter 2001 measured
17 SO₂ concentrations of up to 40 ppb (see [https://www.rap.ucar.edu/asr2002/i-
18 precip_physics/precip_physics.htm](https://www.rap.ucar.edu/asr2002/i-precip_physics/precip_physics.htm)), greater than what has been previously observed over
19 eastern China (Dickerson et al., 2007; He et al., 2012). The largest hotspot observed by the
20 aircraft, near Zirku Island, also appears to be co-located with a hotspot in OMI retrievals. In
21 another study, passive sampling of SO₂ at various locations on Khark Island near the north end
22 of the Gulf during 2003-2004 reported that the SO₂ loading was above the air quality standard
23 (sometimes by several-fold) most of the time (Pourzamani et al., 2012). These high SO₂ columns
24 over the Persian Gulf are likely the result of gas flaring activities from offshore oil and natural
25 gas facilities, although shipping emissions and other sources may also contribute to them. Gas
26 flaring is used on offshore oil rigs to dispose of gases such as hydrogen sulfide (H₂S) for safety,
27 operational, and economic reasons and can have significant impacts on the local and regional
28 environment in the Middle East.

29 Middle East cities also show SO₂ emissions due to both mobile and stationary sources.
30 Oil-burning boilers may constitute another important source of SO₂ in cities or population

1 centers, as implied by the relatively high sulfate ($\sim 10 \mu\text{g m}^{-3}$) that is closely associated with oil
2 combustion tracers (e.g., vanadium), according to an aerosol source apportionment study for
3 Kuwait City (Alolayan et al., 2013). The S content in gasoline and diesel is much higher in this
4 region as compared with others such as Europe, which enforces stricter emission control
5 measures (see [http://www.unep.org/transport/pcf/PDF/JordanWrkshp-
6 MiddleEastFuelQuality.pdf](http://www.unep.org/transport/pcf/PDF/JordanWrkshp-MiddleEastFuelQuality.pdf)). Some of the largest point SO_2 sources in the region coincide with
7 smelters or oil refineries, such as the Sarcheshmeh Copper Complex in Kerman Province, Iran,
8 which is the largest copper smelter in the Middle East. Fig. 3 (bottom row) show interannual
9 variations in observed SO_2 and NO_2 columns over Persian Gulf (blue box in Fig. 7). Since 2010
10 SO_2 columns have steadily dropped by $\sim 20\%$, but increased again in 2014-2015 to 2005 levels.
11 A recent study (Lelieveld et al., 2015) reported that OMI SO_2 over the Persian Gulf increased
12 between 2005 and 2010, and then decreased between 2010 and 2014. Their results are based on
13 retrievals using a different algorithm, but are qualitatively consistent with this study.

14 OMI-retrieved regional NO_2 levels over the Middle East are much smaller than over
15 China (Fig. 6) and the US (Fig. 2). This may also be the results of the short lifetime of NO_2 in
16 this hot and photochemically active region (Beirle et al., 2011). NO_x emissions in the region are
17 associated with power generation and mobile sources. Local NO_2 enhancements coincide with
18 heavily populated cities that have high car densities, such as Jerusalem (Israel) and Cairo (Egypt)
19 (Boersma et al., 2009), Tehran (Iran), Kuwait City (Kuwait), Dubai (UAE), Riyadh and Jeddah
20 (Saudi Arabia). In terms of regional trend over the Persian Gulf (blue box in Fig. 7), NO_2
21 columns increased by $\sim 20\%$ between 2005 and 2008, but remained approximately constant
22 afterwards (Fig. 3). For major metropolitan areas in the region, Lelieveld et al. (2015) focused on
23 the reversal of OMI NO_2 trends due to recent air quality regulations and domestic and
24 international conflicts in the region. Their results are, for the most part, qualitatively consistent
25 with Fig. 7. For example, their reported decrease of NO_2 over Damascus, Syria since 2011 (due
26 to civil war) and increase over Baghdad, Iraq since 2007 are also visible in Fig. 7.

27 **4 Conclusions**

28 The first decade of OMI observations have yielded profound insights into the spatial distribution
29 and temporal trends in SO_2 and NO_2 pollution around the world. For regions with detailed

1 bottom-up emissions estimates or continuous emissions monitoring, OMI shows generally good
2 agreement with these independent data sources. OMI-derived trends also agree well with those
3 from available in situ measurements and deposition data. This adds confidence to the use of OMI
4 to track locations, changes, and transport patterns of SO₂ and NO₂ over areas of the planet
5 lacking local observations. In many regions pollution levels have changed dramatically reflecting
6 underlying changes in SO₂ and NO_x emissions (Fig. 8):

7 1) Over the eastern US, both NO₂ and SO₂ levels decreased dramatically from 2005 to 2015. SO₂
8 concentrations over the Ohio River Valley and western Pennsylvania fell by 80%, consistent
9 with the National Emission Inventory (NEI), which reports a decrease of about 66% for total US
10 emissions. NO₂ concentrations over the eastern US fell by more than 40%, also consistent with
11 the NEI trend for emissions from the entire country. The Clean Air Act Amendments and
12 regulations such as CAIR mandated these emissions reductions, and OMI confirmed their
13 efficacy.

14 2) Over eastern Europe, OMI observed substantial (more than 50%) SO₂ decreases in the vicinity
15 of the largest coal-fired power plants, where flue gas desulfurization devices were installed
16 during the study period. Over some areas including Turkey and Serbia, local SO₂ increased,
17 perhaps because of increased industrial activity. NO₂ levels in the vicinity of the largest eastern
18 European power plants in Bulgaria remain constant.

19 3) Over China, the highest SO₂ and NO₂ levels are observed over the North China Plain, with the
20 highest concentrations in the world. SO₂ peaked in 2007, with a secondary peak in 2011, but by
21 2015 SO₂ has fallen to half of the levels seen at the beginning of the OMI record in 2005. Total
22 Chinese electricity production and coal combustion have increased during the same period, and
23 the observed decrease likely has resulted from centralization of industry and power production
24 and the implementation of pollution control devices. NO₂ concentrations peaked in 2011, but by
25 2015 have returned to 2005 levels.

26 4) Over India, despite relatively low levels as compared with China, both SO₂ and NO₂ have
27 increased, particularly over the northeast, where a large number of newly built coal power plants
28 have doubled SO₂ while increasing NO₂ by ~50%. This is the fastest increase in pollution

1 concentrations observed by OMI. In 2014 India has surpassed the US to become the world's
2 second largest SO₂ emitting country.

3 5) Over the Middle East, OMI detected several SO₂ hot spots with a broad maximum over the
4 Persian Gulf region. These hotspots are probably related to oil and gas operations but are mostly
5 absent in bottom-up emission inventories, such as EDGAR. High concentrations of NO₂ are
6 observed over major cities but less so over oil and gas operations. SO₂ shows no discernable
7 trend over the Gulf while NO₂ rose from 2005 to 2008 and has since remained largely
8 unchanged.

9 In summary, this study demonstrates that satellite remote sensing from advanced
10 instruments such as OMI can provide long-term, nearly continuous global monitoring of SO₂ and
11 NO₂. Where *in situ* concentration measurements, emission inventories, and deposition
12 monitoring are available, OMI provides complementary measurements to supplement and verify
13 those other data sources. OMI can also find unreported or underreported major emissions such
14 as over the Persian Gulf. OMI SO₂ and NO₂ data can also help to further our understanding of
15 the production and impact of secondary pollutants such as tropospheric ozone and particulate
16 matter. Better understanding of these secondary pollutants will help refining satellite SO₂ and
17 NO₂ retrievals.

18 Space-based monitoring plays an increasingly important role in the science of
19 tropospheric chemistry and air quality applications to help mitigate anthropogenic and natural
20 impacts on climate, sensitive ecosystems, and human health. It is essential to continue and
21 maintain overlapping long-term satellite data records. The baseline established during the first 11
22 years of OMI is invaluable for the interpretation of measurements from future satellite
23 atmospheric chemistry missions. The OMI NO₂ and SO₂ data sets used in this study will be
24 refined and continued by the TROPOspheric Monitoring Instrument (TROPOMI) (Veefkind et
25 al., 2012), which is planned for launch on ESA's Sentinel 5 Precursor (S5P) satellite in 2016.
26 TROPOMI will have a significantly higher signal-to-noise and spatial resolution (7km x 7km at
27 nadir) than OMI; both features are very important for monitoring point pollution sources and
28 trends. TROPOMI is part of the European Sentinel series that will continue the global pollution
29 data record for another 20 years (Ingmann et al., 2012). The space-based capabilities for air
30 quality applications will be further enhanced by the addition of higher-ground resolution hourly

1 observations from the three geostationary satellites over North America (Tropospheric
2 emissions: monitoring of pollution (TEMPO), <http://tempo.si.edu>) (Chance et al., 2013), over
3 Europe (Sentinel 4 UVN (Ingmann et al., 2012)) and East Asia (Geostationary Environment
4 Monitoring Spectrometer (GEMS) on board the GeoKOMPSAT satellite) (Kim, 2012). This
5 constellation will allow for unprecedented observations of the key pollutants in the atmosphere.

6

7

8

9 **Appendix A: Filtering transient volcanic clouds**

10 Days affected by transient volcanic SO₂ signals were excluded as follows. Every day the
11 region-wide 99.9-percentile of SO₂ VCDs was computed. If it was found to exceed a threshold
12 value (Table A1) then all data from that day were excluded. This was found to perform better
13 than a simple maximum SO₂ or NO₂ column cut-off as it tended to remove volcanic signals that,
14 while elevated, would not exceed the maximum. A disadvantage of this method is that, while the
15 volcanic contamination would generally only impact a small portion of the region, all data from
16 that day were removed. The SO₂ threshold employed varied from 5 to 10 DU (table A1) and was
17 chosen by examining the 99.9-percentile time series during known periods of minimal volcanic
18 activity. Different regions were found to be affected differently, a result of their proximity to
19 significant eruptions. For regions that span the northern mid-latitudes such as US, Europe, and
20 China, many of the days occurred in 2008 and 2009 and can be attributed to the eruptions of
21 Kasatochi (Aleutian Islands, Alaska, August 2008, 52N) and Sarychev (Kuril Islands, Eastern
22 Russia, June 2009, 48N). By contrast, the Nabro eruption (northern Africa, June 2011, 13.37N)
23 removed the most days over India and Africa whereas the Middle East appeared to be largely
24 unaffected by volcanic emissions.

25 **Appendix B: Timeseries analysis**

26 We use standard Level 3 monthly regional mean SO₂ and NO₂ columns and a regression model
27 discussed in Lamsal et al., (2015) to compare inter-annual timeseries for different regions. The
28 time series of monthly average values (Ω) are assumed to be comprised of three additive

1 subcomponents: a seasonal component (α), a linear trend component (β), and residues or noise
2 (R) component:

$$3 \quad \Omega(t) = \alpha(t) + \beta t + R(t), \quad (\text{B1})$$

4 where, t represents time (month). The time dependent seasonal regression coefficient (α) is given
5 by a constant plus intra-annual sine and cosine harmonic series (Randel and Cobb 1994):

$$6 \quad \alpha(t) = c_0 + \sum_{j=1}^3 \left(c_{1j} \sin\left(\frac{2\pi jt}{12}\right) + c_{2j} \cos\left(\frac{2\pi jt}{12}\right) \right), \quad (\text{B2})$$

7 where c_0, c_{1j} , and c_{2j} are constant coefficients. The major portion of the annual cycle is
8 explained by the seasonal variation of the NO_x and SO_2 lifetime. Other factors, such as monthly
9 variation in source strength, could also affect the annual variation of NO_2 and SO_2 columns, but
10 these contributions, especially for NO_2 , to the seasonal cycle are typically smaller, especially for
11 polluted areas. The seasonal pattern can evolve with time. We identify and extract seasonal and
12 trend components by exploiting changes in the seasonal pattern (amplitude and phase) for
13 individual years. For each year we fit a regression line using monthly observations from that year
14 itself and 6 observations each from adjacent years. This provides a series of local regression lines
15 that incorporate explicit time dependence. Comparison of local regression lines with high- and
16 low-amplitude regression lines allows identification and isolation of two seasonal terms (α_1, α_2 ,
17 where $\alpha = \alpha_1 + \alpha_2$ in Eq. 1) and the linear trend (β) and residues. Since we are interested in
18 interannual changes, we do not explicitly derive linear trend, but rather calculate changes from
19 2005 from de-seasonalized NO_2 and SO_2 columns (Fig. 3).

20 **Acknowledgements**

21 The authors acknowledge the NASA Earth Science Division for funding of OMI SO_2 and NO_2
22 product development and analysis. The Dutch - Finnish built OMI instrument is part of the
23 NASA's EOS Aura satellite payload. We thank systems engineering, instrument calibration and
24 satellite integration teams for making this mission a success. The OMI project is managed by
25 KNMI and the Netherlands Space Agency (NSO). The authors would like to thank the KNMI
26 OMI team for producing L1B radiance and irradiance data and updating the key calibration data,
27 the operational algorithm for the NO_2 slant column fitting and performing operations together

1 with the U.S. Aura operations team, as well as OMI SIPS processing team for continuing
2 support. Authors would like to thank two anonymous reviewers for their helpful comments.

3 **References**

- 4 Ahmad, Z., McClain, C. R., Herman, J. R., Franz, B. A., Kwiatkowska, E. J., Robinson, W. D.,
5 Bucsela, E. J. and Tzortziou, M.: Atmospheric correction for NO₂ absorption in retrieving water-
6 leaving reflectances from the SeaWiFS and MODIS measurements., *Appl. Opt.*, 46(26), 6504–
7 6512, doi:10.1364/AO.46.006504, 2007.
- 8 Alolayan, M. A., Brown, K. W., Evans, J. S., Bouhamra, W. S. and Koutrakis, P.: Source
9 apportionment of fine particles in Kuwait City., *Sci. Total Environ.*, 448, 14–25,
10 doi:10.1016/j.scitotenv.2012.11.090, 2013.
- 11 AQ_Environment_EC: Air Quality - Environment - European Commission, [online] Available
12 from: http://ec.europa.eu/environment/air/quality/legislation/time_extensions.htm (Accessed 18
13 August 2015), 2015.
- 14 ARP: Acid Rain Program | Clean Air Markets | US Environmental Protection Agency, EPA
15 [online] Available from: <http://www.epa.gov/airmarkets/> (Accessed 7 March 2016), 2016.
- 16 Beirle, S., Boersma, K. F., Platt, U., Lawrence, M. G. and Wagner, T.: Megacity emissions and
17 lifetimes of nitrogen oxides probed from space., *Science*, 333(6050), 1737–9,
18 doi:10.1126/science.1207824, 2011.
- 19 Boersma, K. F., Jacob, D. J., Eskes, H. J., Pinder, R. W., Wang, J. and van der A, R. J.:
20 Intercomparison of SCIAMACHY and OMI tropospheric NO₂ columns: Observing the diurnal
21 evolution of chemistry and emissions from space, *J. Geophys. Res. Atmos.*, 113(16),
22 doi:10.1029/2007JD008816, 2008.
- 23 Boersma, K. F., Jacob, D. J., Trainic, M., Rudich, Y., Desmedt, I., Dirksen, R. and Eskes, H. J.:
24 Validation of urban NO₂ concentrations and their diurnal and seasonal variations observed from
25 the SCIAMACHY and OMI sensors using in situ surface measurements in Israeli cities, *Atmos.*
26 *Chem. Phys.*, 9(2), 3867–3879, doi:10.5194/acp-9-3867-2009, 2009.
- 27 Boersma, K. F., Eskes, H. J., Dirksen, R. J., Van Der A, R. J., Veefkind, J. P., Stammes, P.,
28 Huijnen, V., Kleipool, Q. L., Sneep, M., Claas, J., Leitão, J., Richter, A., Zhou, Y. and Brunner,
29 D.: An improved tropospheric NO₂ column retrieval algorithm for the Ozone Monitoring
30 Instrument, *Atmos. Meas. Tech.*, 4(9), 1905–1928, doi:10.5194/amt-4-1905-2011, 2011.
- 31 Boersma, K. F., Vinken, G. C. M. and Tournadre, J.: Ships going slow in reducing their NO_x
32 emissions: changes in 2005–2012 ship exhaust inferred from satellite measurements over
33 Europe, *Environ. Res. Lett.*, 10(7), 074007, doi:10.1088/1748-9326/10/7/074007, 2015.
- 34 Bovensmann, H., Burrows, J. P., Buchwitz, M., Frerick, J., Noël, S., Rozanov, V. V., Chance, K.
35 V. and Goede, a. P. H.: SCIAMACHY: Mission Objectives and Measurement Modes, *J. Atmos.*
36 *Sci.*, 56(2), 127–150, doi:10.1175/1520-0469, 1999.
- 37 Bucsela, E. J., Krotkov, N. A., Celarier, E. A., Lamsal, L. N., Swartz, W. H., Bhartia, P. K.,
38 Boersma, K. F., Veefkind, J. P., Gleason, J. F. and Pickering, K. E.: A new stratospheric and
39 tropospheric NO₂ retrieval algorithm for nadir-viewing satellite instruments: applications to
40 OMI, *Atmos. Meas. Tech.*, 6(1), 2607–2626, doi:10.5194/amt-6-2607-2013, 2013.

1 Burrows, J. P., Buchwitz, M., Rozanov, V., Weber, M., Richter, A., Ladstätter-Weissenmayer, A.
2 and Eisinger, M.: The Global Ozone Monitoring Experiment (GOME): Mission, instrument
3 concept, and first scientific results, Eur. Sp. Agency, (Special Publ. ESA SP, (414 PART 2),
4 585–590, doi:10.1175/1520-0469, 1997.

5 Burrows, J. P., Weber, M., Buchwitz, M., Rozanov, V. and Ladst, A.: The Global Ozone
6 Monitoring Experiment (GOME): Mission Concept and First Scientific Results Corresponding
7 Author :, J. Atmos. Sci., 56(2), 151–175, doi:10.1175/1520-0469, 1999.

8 CAAA: EPA History: Clean Air Act Amendments of 1990, [online] Available from:
9 <http://www2.epa.gov/aboutepa/epa-history-clean-air-act-amendments-1990> (Accessed 7 March
10 2016), 1990.

11 CAIR: Programs | Clean Air Markets | US Environmental Protection Agency, [online] Available
12 from: <http://www.epa.gov/airmarkets/programs/> (Accessed 7 March 2016), 2009.

13 Callies, J., Corpaccioli, E., Eisinger, M., Hahne, A., and Lefebvre, A.: GOME-2 - Metop's
14 second-generation sensor for operational ozone monitoring, ESA Bull. Sp. Agency, 102(may),
15 28–36, Available from: <http://www.esa.int/esapub/bulletin/bullet102/Callies102.pdf> (Accessed 7
16 March 2016), 2000.

17 Carn, S. A., Krueger, A. J., Krotkov, N. A., and Gray, M. A.: Fire at Iraqi sulfur plant emits SO₂
18 clouds detected by Earth Probe TOMS, Geophys. Res. Lett., 31(19), 2–5,
19 doi:10.1029/2004GL020719, 2004.

20 Carn, S. A., Krueger, A. J., Krotkov, N. A., Yang, K. and Levelt, P. F.: Sulfur dioxide emissions
21 from Peruvian copper smelters detected by the Ozone Monitoring Instrument, Geophys. Res.
22 Lett., 34(9), doi:10.1029/2006GL029020, 2007.

23 Castellanos, P. and Boersma, K. F.: Reductions in nitrogen oxides over Europe driven by
24 environmental policy and economic recession., Sci. Rep., 2, 265, doi:10.1038/srep00265, 2012.

25 Castellanos, P., Marufu, L. T., Doddridge, B. G., Taubman, B. F., Schwab, J. J., Hains, J. C.,
26 Ehrman, S. H. and Dickerson, R. R.: Ozone, oxides of nitrogen, and carbon monoxide during
27 pollution events over the eastern United States: An evaluation of emissions and vertical mixing,
28 J. Geophys. Res., 116(D16), D16307, doi:10.1029/2010JD014540, 2011.

29 Castellanos, P., Boersma, K. F. and van der Werf, G. R.: Satellite observations indicate
30 substantial spatiotemporal variability in biomass burning NO_x emission factors for South
31 America, Atmos. Chem. Phys., 14(8), 3929–3943, doi:10.5194/acp-14-3929-2014, 2014.

32 Chance, K., Liu, X., Suleiman, R. M., Flittner, D. E., Al-Saadi, J. and Janz, S. J.: Tropospheric
33 emissions: monitoring of pollution (TEMPO), SPIE Opt. Eng. + Appl., 8866 (Sentinel 4),
34 88660D, doi:10.1117/12.2024479, 2013.

35 Chance, K. V. and Spurr, R. J. D.: Ring effect studies: Rayleigh scattering, including molecular
36 parameters for rotational Raman scattering, and the Fraunhofer spectrum, Appl. Opt., 36, 5224–
37 5230, doi:10.1364/AO.36.005224, 1997.

38 Chubarova, N. Y., Larin, L. K., Lebedev, V. V., Partola, V. S., Lezina, Y. A. and Rublev, A. N.:
39 Experimental and model study of changes in spectral solar irradiance in the atmosphere of large
40 city due to tropospheric NO₂ content, Curren Probl. Atmos. Radiat. (IRS 2008) Ed. by T.
41 Nakajima M.A. Yamasoe, AIP Conf. Proc., 1100(2), 459–462, doi:10.1063/1.3117019, 2009.

42 Chubarova, N. Y., Poliukhov, A. A. and Gorlova, I. D.: Long-term variability of aerosol optical

1 thickness in Eastern Europe over 2001–2014 according to the measurements at the Moscow MSU
2 MO AERONET site with additional cloud and NO₂ correction, *Atmos. Meas. Tech.*, 9(2), 313–
3 334, doi:10.5194/amt-9-313-2016, 2016.

4 Curier, R. L., Kranenburg, R., Segers, A. J. S., Timmermans, R. M. A. and Schaap, M.:
5 Synergistic use of OMI NO₂ tropospheric columns and LOTOS–EUROS to evaluate the NO_x
6 emission trends across Europe, *Remote Sens. Environ.*, 149, 58–69,
7 doi:10.1016/j.rse.2014.03.032, 2014.

8 Denby, B., Sundvor, I., Cassiani, M., de Smet, P., de Leeuw, F. and Horálek, J.: Spatial mapping
9 of ozone and SO₂ trends in Europe., *Sci. Total Environ.*, 408(20), 4795–806,
10 doi:10.1016/j.scitotenv.2010.06.021, 2010.

11 Dickerson, R. R.: Analysis of black carbon and carbon monoxide observed over the Indian
12 Ocean: Implications for emissions and photochemistry, *J. Geophys. Res.*, 107(D19), 8017,
13 doi:10.1029/2001JD000501, 2002.

14 Dickerson, R. R., Li, C., Li, Z., Marufu, L. T., Stehr, J. W., McClure, B., Krotkov, N., Chen, H.,
15 Wang, P., Xia, X., Ban, X., Gong, F., Yuan, J. and Yang, J.: Aircraft observations of dust and
16 pollutants over northeast China: Insight into the meteorological mechanisms of transport, *J.*
17 *Geophys. Res. Atmos.*, 112(24), 1–13, doi:10.1029/2007JD008999, 2007.

18 Ding, J., van der A, R. J., Mijling, B., Levelt, P. F. and Hao, N.: NO_x emission estimates during
19 the 2014 Youth Olympic Games in Nanjing, *Atmos. Chem. Phys.*, 15, 9399–9412,,
20 doi:10.5194/acp-15-9399-2015, 2015.

21 Dittman, M. G., Ramberg, E., Chrisp, M., Rodriguez, J. V., Sparks, A. L., Zaun, N. H.,
22 Hendershot, P., Dixon, T., Philbrick, R. H. and Wasinger, D.: Nadir ultraviolet imaging
23 spectrometer for the NPOESS Ozone Mapping and Profiler Suite (OMPS), *Earth Observing*
24 *Systems VII*, William L. Barnes, Editor, *Proceedings of SPIE Vol. 4814*, 2002.

25 Dobber, M. R., Dirksen, R. J., Levelt, P. F., Oord, G. H. J. Van Den, Voors, R. H. M., Kleipool,
26 Q., Jaross, G., Kowalewski, M., Hilsenrath, E., Leppelmeier, G. W., Vries, J. D. V. J. De,
27 Dierssen, W. and Rozemeijer, N. C.: Ozone monitoring instrument calibration, *IEEE Trans.*
28 *Geosci. Remote Sens.*, 44(5), 1209–1238, doi:10.1109/TGRS.2006.869987, 2006.

29 Duncan, B. N., Yoshida, Y., Olson, J. R., Sillman, S., Martin, R. V., Lamsal, L., Hu, Y.,
30 Pickering, K. E., Retscher, C., Allen, D. J. and Crawford, J. H.: Application of OMI observations
31 to a space-based indicator of NO_x and VOC controls on surface ozone formation, *Atmos.*
32 *Environ.*, 44(18), 2213–2223, doi:10.1016/j.atmosenv.2010.03.010, 2010.

33 Duncan, B. N., Yoshida, Y., de Foy, B., Lamsal, L. N., Streets, D. G., Lu, Z., Pickering, K. E.
34 and Krotkov, N. A.: The observed response of Ozone Monitoring Instrument (OMI) NO₂
35 columns to NO_x emission controls on power plants in the United States: 2005–2011, *Atmos.*
36 *Environ.*, 81, 102–111, doi:10.1016/j.atmosenv.2013.08.068, 2013.

37 Duncan, B. N., Prados, A. I., Lamsal, L. N., Liu, Y., Streets, D. G., Gupta, P., Hilsenrath, E.,
38 Kahn, R. A., Nielsen, J. E., Beyersdorf, A. J., Burton, S. P., Fiore, A. M., Fishman, J., Henze, D.
39 K., Hostetler, C. A., Krotkov, N. A., Lee, P., Lin, M., Pawson, S., Pfister, G., Pickering, K. E.,
40 Pierce, R. B., Yoshida, Y. and Ziemba, L. D.: Satellite data of atmospheric pollution for U.S. air
41 quality applications: Examples of applications, summary of data end-user resources, answers to
42 FAQs, and common mistakes to avoid, *Atmos. Environ.*, 94, 647–662,
43 doi:10.1016/j.atmosenv.2014.05.061, 2014.

1 Duncan, B. N., Lamsal, L. N., Thompson, A. M., Yoshida, Y., Lu, Z., Streets, D. G., Hurwitz,
2 M. M. and Pickering, K. E.: A space-based, high-resolution view of notable changes in urban
3 NO_x pollution around the world (2005-2014), *J. Geophys. Res. Atmos.*, 121(2), 976–996,
4 doi:10.1002/2015JD024121, 2016.

5 EEA: European Union emission inventory report 1990–2011 under the UNECE Convention on
6 Long-range Transboundary Air Pollution (LRTAP), European Environment Agency (EEA),
7 Technical report No 10/2013, doi:10.2800/44480, 2013.

8 Eisinger, M. and Burrows, J. P.: Tropospheric sulfur dioxide observed by the ERS-2 GOME
9 instrument, *Geophys. Res. Lett.*, 25(22), 4177–4180, doi:10.1029/1998GL900128, 1998.

10 Elansky, N. F., Lokoshchenko, M. a., Belikov, I. B., Skorokhod, a. I. and Shumskii, R. a.:
11 Variability of trace gases in the atmospheric surface layer from observations in the city of
12 Moscow, *Izv. Atmos. Ocean. Phys.*, 43(2), 219–231, doi:10.1134/S0001433807020089, 2007.

13 EPA: Reactive Nitrogen in the United States: An Analysis of Inputs, Flows, Consequences, and
14 Management Options, Washington, DC. [online] Available from:
15 [http://yosemite.epa.gov/sab/sabproduct.nsf/WebBOARD/INCFullReport/\\$File/Final INC](http://yosemite.epa.gov/sab/sabproduct.nsf/WebBOARD/INCFullReport/$File/Final%20INC%20Report_8_19_11(without%20signatures).pdf)
16 [Report_8_19_11\(without signatures\).pdf](http://yosemite.epa.gov/sab/sabproduct.nsf/WebBOARD/INCFullReport/$File/Final INC Report_8_19_11(without signatures).pdf) (Accessed 7 March 2016), 2011.

17 EPA: Integrated Science Assessment of Ozone and Related Photochemical Oxidants, [online]
18 Available from: <http://cfpub.epa.gov/ncea/isa/recordisplay.cfm?deid=247492#Download>
19 (Accessed 7 March 2016), 2013.

20 European Commission: Air Quality Standards - Environment - European Commission, [online]
21 Available from: <http://ec.europa.eu/environment/air/quality/standards.htm> (Accessed 7 March
22 2017), 2015.

23 Fioletov, V., McLinden, C., Krotkov, N. A. and Li, C.: A global catalogue of SO₂ sources and
24 emissions derived from Ozone Monitoring Instrument, prepared for *Atmos. Chem. Phys.*, 2016.

25 Fioletov, V. E., McLinden, C. A., Krotkov, N., Moran, M. D. and Yang, K.: Estimation of SO₂
26 emissions using OMI retrievals, *Geophys. Res. Lett.*, 38(21), doi:10.1029/2011GL049402, 2011.

27 Fioletov, V. E., McLinden, C. a., Krotkov, N., Yang, K., Loyola, D. G., Valks, P., Theys, N.,
28 Van Roozendaal, M., Nowlan, C. R., Chance, K., Liu, X., Lee, C. and Martin, R. V.: Application
29 of OMI, SCIAMACHY, and GOME-2 satellite SO₂ retrievals for detection of large emission
30 sources, *J. Geophys. Res. Atmos.*, 118(19), 11399–11418, doi:10.1002/jgrd.50826, 2013.

31 Fioletov, V. E., McLinden, C. A., Krotkov, N. and Li, C.: Lifetimes and emissions of SO₂ from
32 point sources estimated from OMI, *Geophys. Res. Lett.*, 42(6), 1969–1976,
33 doi:10.1002/2015GL063148, 2015.

34 Flynn, L., Long, C., Wu, X., Evans, R., Beck, C. T., Petropavlovskikh, I., McConville, G., Yu,
35 W., Zhang, Z., Niu, J., Beach, E., Hao, Y., Pan, C., Sen, B., Novicki, M., Zhou, S. and Seftor, C.:
36 Performance of the Ozone Mapping and Profiler Suite (OMPS) products, *J. Geophys. Res.*
37 *Atmos.*, 119(10), 6181–6195, doi:10.1002/2013JD020467, 2014.

38 de Foy, B., Krotkov, N. A., Bei, N., Herndon, S. C., Huey, L. G., Martínez, A.-P., Ruiz-Suárez,
39 L. G., Wood, E. C., Zavala, M. and Molina, L. T.: Hit from both sides: tracking industrial and
40 volcanic plumes in Mexico City with surface measurements and OMI SO₂ retrievals during the
41 MILAGRO field campaign, *Atmos. Chem. Phys.*, 9(24), 9599–9617, doi:10.5194/acp-9-9599-
42 2009, 2009.

1 de Foy, B., Wilkins, J. L., Lu, Z., Streets, D. G. and Duncan, B. N.: Model evaluation of methods
2 for estimating surface emissions and chemical lifetimes from satellite data, *Atmos. Environ.*, 98,
3 66–77, doi:10.1016/j.atmosenv.2014.08.051, 2014.

4 de Foy, B., Lu, Z., Streets, D. G., Lamsal, L. N. and Duncan, B. N.: Estimates of power plant
5 NO_x emissions and lifetimes from OMI NO₂ satellite retrievals, *Atmos. Environ.*, 116, 1–11,
6 doi:10.1016/j.atmosenv.2015.05.056, 2015.

7 Frost, G. J., McKeen, S. A., Trainer, M., Ryerson, T. B., Neuman, J. A., Roberts, J. M.,
8 Swanson, A., Holloway, J. S., Sueper, D. T., Fortin, T., Parrish, D. D., Fehsenfeld, F. C., Flocke,
9 F., Peckham, S. E., Grell, G. A., Kowal, D., Cartwright, J., Auerbach, N. and Habermann, T.:
10 Effects of changing power plant NO_x emissions on ozone in the eastern United States: Proof of
11 concept, *J. Geophys. Res.*, 111(D12), D12306, doi:10.1029/2005JD006354, 2006.

12 Galloway, J. N., Leach, A. M., Bleeker, A. and Erisman, J. W.: A chronology of human
13 understanding of the nitrogen cycle, *Philos. Trans. R. Soc. London B Biol. Sci.*, 368(1621)
14 [online] Available from:
15 <http://rstb.royalsocietypublishing.org/content/368/1621/20130120.abstract> , 2013.

16 Geddes, J. A., Murphy, J. G., O'Brien, J. M. and Celarier, E. A.: Biases in long-term NO₂
17 averages inferred from satellite observations due to cloud selection criteria, *Remote Sens.*
18 *Environ.*, 124, 210–216, doi:10.1016/j.rse.2012.05.008, 2012.

19 Ghude, S. D., Lal, D. M., Beig, G., Van Der A, R. and Sable, D.: Rain-induced soil NO_x
20 emission from India during the onset of the summer monsoon: A satellite perspective, *J.*
21 *Geophys. Res. Atmos.*, 115(16), doi:10.1029/2009JD013367, 2010.

22 Ghude, S. D., Kulkarni, P. S., Kulkarni, S. H., Fadnavis, S. and Van Der A, R. J.: Temporal
23 variation of urban NO_x concentration in India during the past decade as observed from space,
24 *Int. J. Remote Sens.*, 32(3), 849–861, doi:10.1080/01431161.2010.517797, 2011.

25 Ghude, S. D., Pfister, G. G., Jena, C., Van Der A, R. J., Emmons, L. K. and Kumar, R.: Satellite
26 constraints of nitrogen oxide (NO_x) emissions from India based on OMI observations and WRF-
27 Chem simulations, *Geophys. Res. Lett.*, 40(2), 423–428, doi:10.1029/2012GL053926, 2013.

28 Gorchakov, G., Semoutnikova, E., Karpov, A., and Lezina, E.: Air Pollution in Moscow
29 Megacity, Chapter 11, in: *Advanced Topics in Environmental Health and Air Pollution Case*
30 *Studies*, edited by Moldoveanu, A. M., InTech., 2011.

31 Guay, J.: China's Thirst for Coal Is Drying Up, [online] Available from:
32 http://www.huffingtonpost.com/justin-guay/chinas-thirst-for-coal-is_b_5358194.html (Accessed
33 7 March 2016), 2015.

34 Hand, J. L., Schichtel, B. A., Malm, W. C. and Pitchford, M. L.: Particulate sulfate ion
35 concentration and SO₂ emission trends in the United States from the early 1990s through 2010,
36 *Atmos. Chem. Phys.*, 12(21), 10353–10365, doi:10.5194/acp-12-10353-2012, 2012.

37 Hayn, M., Beirle, S., Hamprecht, F. A., Platt, U., Menze, B. H. and Wagner, T.: Analysing
38 spatio-temporal patterns of the global NO₂-distribution retrieved from GOME satellite
39 observations using a generalized additive model, *Atmos. Chem. Phys.*, 9(17), 6459–6477,
40 doi:10.5194/acp-9-6459-2009, 2009.

41 He, H., Li, C., Loughner, C. P., Li, Z., Krotkov, N. A., Yang, K., Wang, L., Zheng, Y., Bao, X.,
42 Zhao, G. and Dickerson, R. R.: SO₂ over central China : Measurements, numerical simulations

1 and the tropospheric sulfur budget, , 117, 1–15, doi:10.1029/2011JD016473, 2012.

2 He, H., Vinnikov, K., Li, C., Krotkov, N. A., Jongeward, A. R., Li, Z., Stehr, J. W., Hains, J. C.
3 and Dickerson, R. R.: Response of SO₂ and particulate air pollution to local and regional
4 emission controls: A case study in Maryland, under review, *Earth's Future*, 2016.

5 Herman, J., Deland, M. T., Huang, L. K., Labow, G., Larko, D., Lloyd, S. A., Mao, J., Qin, W.
6 and Weaver, C.: A net decrease in the Earth's cloud, aerosol, and surface 340 nm reflectivity
7 during the past 33 yr (1979–2011), *Atmos. Chem. Phys.*, 13(16), 8505–8524, doi:10.5194/acp-
8 13-8505-2013, 2013.

9 Hilboll, A., Richter, A. and Burrows, J. P.: Long-term changes of tropospheric NO₂ over
10 megacities derived from multiple satellite instruments, *Atmos. Chem. Phys.*, 13(8), 4145–4169,
11 doi:10.5194/acp-13-4145-2013, 2013.

12 Hogrefe, C., Hao, W., Zalewsky, E. E., Ku, J.-Y., Lynn, B., Rosenzweig, C., Schultz, M. G.,
13 Rast, S., Newchurch, M. J., Wang, L., Kinney, P. L. and Sistla, G.: An analysis of long-term
14 regional-scale ozone simulations over the Northeastern United States: variability and trends,
15 *Atmos. Chem. Phys.*, 11(2), 567–582, doi:10.5194/acp-11-567-2011, 2011.

16 Huang, J., Zhou, C., Lee, X., Bao, Y., Zhao, X., Fung, J., Richter, A., Liu, X. and Zheng, Y.: The
17 effects of rapid urbanization on the levels in tropospheric nitrogen dioxide and ozone over East
18 China, *Atmos. Environ.*, 77, 558–567, doi:10.1016/j.atmosenv.2013.05.030, 2013.

19 Ialongo, I., Hakkarainen, J., Kivi, R., Anttila, P., Krotkov, N. A., Yang, K., Li, C., Tukiainen, S.,
20 Hassinen, S. and Tamminen, J.: Comparison of operational satellite SO₂ products with ground-
21 based observations in northern Finland during the Icelandic Holuhraun fissure eruption, *Atmos.*
22 *Meas. Tech.*, 8(6), 2279–2289, doi:10.5194/amt-8-2279-2015, 2015.

23 Ingmann, P., Veihelmann, B., Langen, J., Lamarre, D., Stark, H. and Courrèges-Lacoste, G. B.:
24 Requirements for the GMES Atmosphere Service and ESA's implementation concept: Sentinels-
25 4/-5 and -5p, *Remote Sens. Environ.*, 120, 58–69, doi:10.1016/j.rse.2012.01.023, 2012.

26 IPCC Working Group I, I., Stocker, T. F., Qin, D., Plattner, G.-K., Tignor, M., Allen, S. K.,
27 Boschung, J., Nauels, A., Xia, Y., Bex, V. and Midgley, P. M.: IPCC, 2013: Climate Change
28 2013: The Physical Science Basis. Contribution of Working Group I to the Fifth Assessment
29 Report of the Intergovernmental Panel on Climate Change, IPCC, AR5, 1535, 2013.

30 Irie, H., Boersma, K. F., Kanaya, Y., Takashima, H., Pan, X. and Wang, Z. F.: Quantitative bias
31 estimates for tropospheric NO₂ columns retrieved from SCIAMACHY, OMI, and GOME-2
32 using a common standard for East Asia, *Atmos. Meas. Tech.*, 5(10), 2403–2411,
33 doi:10.5194/amt-5-2403-2012, 2012.

34 Janssens-Maenhout, G., Crippa, M., Guizzardi, D., Dentener, F., Muntean, M., Pouliot, G.,
35 Keating, T., Zhang, Q., Kurokawa, J., Wankmüller, R., Denier van der Gon, H., Kuenen, J. J. P.,
36 Klimont, Z., Frost, G., Darras, S., Koffi, B. and Li, M.: HTAP_v2.2: a mosaic of regional and
37 global emission grid maps for 2008 and 2010 to study hemispheric transport of air pollution,
38 *Atmos. Chem. Phys.*, 15(19), 11411–11432, doi:10.5194/acp-15-11411-2015, 2015.

39 Jia, B., Wang, Y., Yao, Y. and Xie, Y.: A new indicator on the impact of large-scale circulation
40 on wintertime particulate matter pollution over China, *Atmos. Chem. Phys.*, 15, 11919–11929,
41 doi:10.5194/acp-15-11919-2015, 2015.

42 Khokhar, M. F., Frankenberg, C., Van Roozendaal, M., Beirle, S., Köhl, S., Richter, A., Platt, U.

1 and Wagner, T.: Satellite observations of atmospheric SO₂ from volcanic eruptions during the
2 time-period of 1996-2002, in *Advances in Space Research*, vol. 36, pp. 879–887., 2005.

3 Kim, J.: GEMS(Geostationary Environment Monitoring Spectrometer) onboard the
4 GeoKOMPSAT to Monitor Air Quality in high Temporal and Spatial Resolution over Asia-
5 Pacific Region, EGU Gen. Assem. 2012 [online] Available from:
6 <http://adsabs.harvard.edu/abs/2012EGUGA..14.4051K> (Accessed 7 March 2016), 2012.

7 Kim, S. W., Heckel, A., Frost, G. J., Richter, A., Gleason, J., Burrows, J. P., McKeen, S., Hsie,
8 E. Y., Granier, C. and Trainer, M.: NO₂ columns in the western United States observed from
9 space and simulated by a regional chemistry model and their implications for NO_x emissions, *J.*
10 *Geophys. Res. Atmos.*, 114(11), doi:10.1029/2008JD011343, 2009.

11 Klimont, Z., Cofala, J., Xing, J., Wei, W., Zhang, C., Wang, S., Kejun, J., Bhandari, P., Mathur,
12 R., Purohit, P., Rafaj, P., Chambers, A., Amann, M. and Hao, J.: Projections of SO₂, NO_x and
13 carbonaceous aerosols emissions in Asia, *Tellus B*, 61(4), doi:10.3402/tellusb.v61i4.16858,
14 2009.

15 Klimont, Z., Smith, S. J. and Cofala, J.: The last decade of global anthropogenic sulfur dioxide:
16 2000–2011 emissions, *Environ. Res. Lett.*, 8(1), 014003, doi:10.1088/1748-9326/8/1/014003,
17 2013.

18 KNMI: Background information about the Row Anomaly in OMI, [online] Available from:
19 <http://www.knmi.nl/omi/research/product/rowanomaly-background.php> (Accessed 7 March
20 2016), 2012.

21 Konovalov, I. B., Beekmann, M., Richter, A. and Burrows, J. P.: Inverse modelling of the spatial
22 distribution of NO_x emissions on a continental scale using satellite data, *Atmos. Chem. Phys.*,
23 6(7), 1747–1770, doi:10.5194/acp-6-1747-2006, 2006.

24 Konovalov, I. B., Beekmann, M., Richter, A., Burrows, J. P. and Hilboll, A.: Multi-annual
25 changes of NO_x emissions in megacity regions: Nonlinear trend analysis of satellite
26 measurement based estimates, *Atmos. Chem. Phys.*, 10(17), 8481–8498, doi:10.5194/acp-10-
27 8481-2010, 2010.

28 Krotkov, N. A., Cam, S. A., Krueger, A. J., Bhartia, P. K. and Yang, K.: Band residual difference
29 algorithm for retrieval of SO₂ from the Aura Ozone Monitoring Instrument (OMI), *IEEE Trans.*
30 *Geosci. Remote Sens.*, 44(5), 1259–1266, doi:10.1109/TGRS.2005.861932, 2006.

31 Krotkov, N. A., McClure, B., Dickerson, R. R., Carn, S. A., Li, C., Bhartia, P. K., Yang, K.,
32 Krueger, A. J., Li, Z., Levelt, P. F., Chen, H., Wang, P. and Lu, D.: Validation of SO₂ retrievals
33 from the Ozone Monitoring Instrument over NE China, *J. Geophys. Res. Atmos.*, 113(16),
34 doi:10.1029/2007JD008818, 2008.

35 Krueger, A. J.: Sighting of el chichon sulfur dioxide clouds with the nimbus 7 total ozone
36 mapping spectrometer., *Science*, 220(4604), 1377–9, doi:10.1126/science.220.4604.1377, 1983.

37 Lamsal, L. N., Martin, R. V., van Donkelaar, A., Steinbacher, M., Celarier, E. A., Bucsela, E.,
38 Dunlea, E. J. and Pinto, J. P.: Ground-level nitrogen dioxide concentrations inferred from the
39 satellite-borne Ozone Monitoring Instrument, *J. Geophys. Res. Atmos.*, 113(16),
40 doi:10.1029/2007JD009235, 2008.

41 Lamsal, L. N., Martin, R. V., Van Donkelaar, A., Celarier, E. A., Bucsela, E. J., Boersma, K. F.,
42 Dirksen, R., Luo, C. and Wang, Y.: Indirect validation of tropospheric nitrogen dioxide retrieved

1 from the OMI satellite instrument: Insight into the seasonal variation of nitrogen oxides at
2 northern midlatitudes, *J. Geophys. Res. Atmos.*, 115(5), doi:10.1029/2009JD013351, 2010.

3 Lamsal, L. N., Martin, R. V., Padmanabhan, A., van Donkelaar, A., Zhang, Q., Sioris, C. E.,
4 Chance, K., Kurosu, T. P. and Newchurch, M. J.: Application of satellite observations for timely
5 updates to global anthropogenic NO_x emission inventories, *Geophys. Res. Lett.*, 38(5), n/a–n/a,
6 doi:10.1029/2010GL046476, 2011.

7 Lamsal, L. N., Martin, R. V., Parrish, D. D. and Krotkov, N. A.: Scaling relationship for NO₂
8 pollution and urban population size: A satellite perspective, *Environ. Sci. Technol.*, 47(14),
9 7855–7861, doi:10.1021/es400744g, 2013.

10 Lamsal, L. N., Duncan, B. N., Yoshida, Y., Krotkov, N. A., Pickering, K. E., Streets, D. G. and
11 Lu, Z.: U.S. NO₂ trends (2005–2013): EPA Air Quality System (AQS) data versus improved
12 observations from the Ozone Monitoring Instrument (OMI), *Atmos. Environ.*, 110, 130–143,
13 doi:10.1016/j.atmosenv.2015.03.055, 2015.

14 Lee, C., Martin, R. V., Van Donkelaar, A., O’Byrne, G., Krotkov, N., Richter, A., Huey, L. G.
15 and Holloway, J. S.: Retrieval of vertical columns of sulfur dioxide from SCIAMACHY and
16 OMI: Air mass factor algorithm development, validation, and error analysis, *J. Geophys. Res.*
17 *Atmos.*, 114(22), doi:10.1029/2009JD012123, 2009.

18 Lee, C., Martin, R. V., Van Donkelaar, A., Lee, H., Dickerson, R. R., Hains, J. C., Krotkov, N.,
19 Richter, A., Vinnikov, K. and Schwab, J. J.: SO₂ emissions and lifetimes: Estimates from inverse
20 modeling using in situ and global, space-based (SCIAMACHY and OMI) observations, *J.*
21 *Geophys. Res. Atmos.*, 116(6), doi:10.1029/2010JD014758, 2011.

22 Lee, C. J., Martin, R. V., Henze, D. K., Brauer, M., Cohen, A. and Donkelaar, A. Van: Response
23 of Global Particulate-Matter-Related Mortality to Changes in Local Precursor Emissions,
24 *Environ. Sci. Technol.*, 150324080130001, doi:10.1021/acs.est.5b00873, 2015.

25 Lelieveld, J., Beirle, S., Hörmann, C., Stenchikov, G. and Wagner, T.: Abrupt recent trend
26 changes in atmospheric nitrogen dioxide over the Middle East, *Sci. Adv.*, 1(7), 2–6, 2015.

27 Leue, C., Wenig, M., Wagner, T., Klimm, O., Platt, U. and Jähne, B.: Quantitative analysis of
28 NO_x emissions from Global Ozone Monitoring Experiment satellite image sequences, *J.*
29 *Geophys. Res.*, 106(D6), 5493, doi:10.1029/2000JD900572, 2001.

30 Levelt, P. F., Hilsenrath, E., Leppelmeier, G. W., Oord, G. H. J. Van Den, Bhartia, P. K.,
31 Tamminen, J., Haan, J. F. De and Veeffkind, J. P.: Science Objectives of the Ozone Monitoring
32 Instrument, *IEEE Trans. Geosci. Remote Sens.*, 44(5), 1199–1208, 2006a.

33 Levelt, P. F., Oord, G. H. J. Van Den, Dobber, M. R., Mälkki, A., Visser, H., Vries, J. De,
34 Stammes, P., Lundell, J. O. V and Saari, H.: The Ozone Monitoring Instrument, *IEEE Trans.*
35 *Geosci. Remote Sens.*, 44(5), 1093–1101, 2006b.

36 Li, C., Marufu, L. T., Dickerson, R. R., Li, Z., Wen, T., Wang, Y., Wang, P., Chen, H. and Stehr,
37 J. W.: In situ measurements of trace gases and aerosol optical properties at a rural site in northern
38 China during East Asian Study of Tropospheric Aerosols: An International Regional Experiment
39 2005, *J. Geophys. Res.*, 112(D22), D22S04, doi:10.1029/2006JD007592, 2007.

40 Li, C., Zhang, Q., Krotkov, N. A., Streets, D. G., He, K., Tsay, S.-C. and Gleason, J. F.: Recent
41 Large Reduction in Sulfur Dioxide Emissions from Chinese Power Plants Observed by the
42 Ozone Monitoring Instrument, *Geophys. Res. Lett.*, 37, 1–6, doi:10.1029/2010GL042594, 2010.

- 1 Li, C., Joiner, J., Krotkov, N. a. and Bhartia, P. K.: A fast and sensitive new satellite SO₂
2 retrieval algorithm based on principal component analysis: Application to the ozone monitoring
3 instrument, *Geophys. Res. Lett.*, 40(23), 6314–6318, doi:10.1002/2013GL058134, 2013.
- 4 Liu, Y., Chen, X., Huang, S., Tian, L., Lu, Y., Mei, Y., Ren, M., Li, N., Liu, L. and Xiang, H.:
5 Association between air pollutants and cardiovascular disease mortality in Wuhan, China., *Int. J.*
6 *Environ. Res. Public Health*, 12(4), 3506–16, doi:10.3390/ijerph120403506, 2015.
- 7 Lookman, A. A. and Rubin, E. S.: Barriers to adopting least-cost particulate control strategies for
8 Indian power plants, *Energy Policy*, 26(14), 1053–1063, doi:10.1016/S0301-4215(98)00049-4,
9 1998.
- 10 Lu, Z. and Streets, D. G.: Increase in NO_x emissions from Indian thermal power plants during
11 1996-2010: unit-based inventories and multisatellite observations., *Environ. Sci. Technol.*,
12 46(14), 7463–70, doi:10.1021/es300831w, 2012.
- 13 Lu, Z., Streets, D. G., Zhang, Q., Wang, S., Carmichael, G. R., Cheng, Y. F., Wei, C., Chin, M.,
14 Diehl, T. and Tan, Q.: Sulfur dioxide emissions in China and sulfur trends in East Asia since
15 2000, *Atmos. Chem. Phys.*, 10(13), 6311–6331, doi:10.5194/acp-10-6311-2010, 2010.
- 16 Lu, Z., Zhang, Q. and Streets, D. G.: Sulfur dioxide and primary carbonaceous aerosol emissions
17 in China and India, 1996–2010, *Atmos. Chem. Phys.*, 11(18), 9839–9864, doi:10.5194/acp-11-
18 9839-2011, 2011.
- 19 Lu, Z., Streets, D. G., De Foy, B. and Krotkov, N. A.: Ozone monitoring instrument observations
20 of interannual increases in SO₂ emissions from Indian coal-fired power plants during 2005-2012,
21 *Environ. Sci. Technol.*, 47(24), 13993–14000, doi:10.1021/es4039648, 2013.
- 22 Lu, Z., Streets, D. G., de Foy, B., Lamsal, L. N., Duncan, B. N. and Xing, J.: Emissions of
23 nitrogen oxides from US urban areas: estimation from Ozone Monitoring Instrument retrievals
24 for 2005–2014, *Atmos. Chem. Phys.*, 15(18), 10367–10383, doi:10.5194/acp-15-10367-2015,
25 2015.
- 26 Martin, R. V.: Satellite remote sensing of surface air quality, *Atmos. Environ.*, 42(34), 7823–
27 7843, doi:10.1016/j.atmosenv.2008.07.018, 2008.
- 28 Martin, R. V., Chance, K., Jacob, D. J., Kurosu, T. P., Spurr, R. J. D., Bucsela, E., Gleason, J. F.,
29 Palmer, P. I., Bey, I., Fiore, A. M., Li, Q., Yantosca, R. M. and Koelemeijer, R. B. A.: An
30 improved retrieval of tropospheric nitrogen dioxide from GOME, *J. Geophys. Res.*, 107(20),
31 4437, doi:10.1029/2001JD001027, 2002.
- 32 McLinden, C. A., Fioletov, V., Boersma, K. F., Krotkov, N., Sioris, C. E., Veefkind, J. P. and
33 Yang, K.: Air quality over the Canadian oil sands: A first assessment using satellite observations,
34 *Geophys. Res. Lett.*, 39(4), doi:10.1029/2011GL050273, 2012.
- 35 McLinden, C. A., Fioletov, V., Boersma, K. F., Kharol, S. K., Krotkov, N., Lamsal, L., Makar,
36 P. A., Martin, R. V., Veefkind, J. P. and Yang, K.: Improved satellite retrievals of NO₂ and SO₂
37 over the Canadian oil sands and comparisons with surface measurements, *Atmos. Chem. Phys.*,
38 14(7), 3637–3656, doi:10.5194/acp-14-3637-2014, 2014.
- 39 McLinden, C. A., Fioletov, V., Krotkov, N. A., Li, C., Boersma, K. F. and Adams, C.: A Decade
40 of Change in NO₂ and SO₂ over the Canadian Oil Sands As Seen from Space., *Environ. Sci.*
41 *Technol.*, 50(1), 331–7, doi:10.1021/acs.est.5b04985, 2016.
- 42 Mebust, A. K. and Cohen, R. C.: Space-based observations of fire NO_x emission coefficients: a

1 global biome-scale comparison, *Atmos. Chem. Phys.*, 14(5), 2509–2524, doi:10.5194/acp-14-
2 2509-2014, 2014.

3 MEP: The airborne pollution prevention and control action plan, [online] Available from:
4 http://english.mep.gov.cn/News_service/infocus/201309/t20130924_260707.htm (Accessed 7
5 March 2016), 2013.

6 Mijling, B. and Van Der A, R. J.: Using daily satellite observations to estimate emissions of
7 short-lived air pollutants on a mesoscopic scale, *J. Geophys. Res. Atmos.*, 117(17), 1–20,
8 doi:10.1029/2012JD017817, 2012.

9 Mijling, B., van der A, R. J., Boersma, K. F., Van Roozendael, M., De Smedt, I. and Kelder, H.
10 M.: Reductions of NO₂ detected from space during the 2008 Beijing Olympic Games, *Geophys.*
11 *Res. Lett.*, 36(13), L13801, doi:10.1029/2009GL038943, 2009.

12 Miyazaki, K., Eskes, H. J. and Sudo, K.: Global NO_x emission estimates derived from an
13 assimilation of OMI tropospheric NO₂ columns, *Atmos. Chem. Phys.*, 12(5), 2263–2288,
14 doi:10.5194/acp-12-2263-2012, 2012.

15 Napelenok, S. L., Pinder, R. W., Gilliland, A. B. and Martin, R. V.: A method for evaluating
16 spatially-resolved NO_x emissions using Kalman filter inversion, direct sensitivities, and space-
17 based NO₂ observations, *Atmos. Chem. Phys.*, 8(18), 5603–5614, doi:10.5194/acp-8-5603-2008,
18 2008.

19 Nowlan, C. R., Martin, R. V., Philip, S., Lamsal, L. N., Krotkov, N. A., Marais, E. A., Wang, S.
20 and Zhang, Q.: Global dry deposition of nitrogen dioxide and sulfur dioxide inferred from space-
21 based measurements, *Global Biogeochem. Cycles*, 28(10), 1025–1043,
22 doi:10.1002/2014GB004805, 2014.

23 Oetjen, H., Baidar, S., Krotkov, N. a., Lamsal, L. N., Lechner, M. and Volkamer, R.: Airborne
24 MAX-DOAS measurements over California: Testing the NASA OMI tropospheric NO₂ product,
25 *J. Geophys. Res. Atmos.*, 118(13), 7400–7413, doi:10.1002/jgrd.50550, 2013.

26 Pourzamani, H., Aliyan, T. and Daryalal, M.: Evaluation of SO₂ level in the ambient air of
27 Khark Island, *Int. J. Environ. Health Eng.*, 1(1), 39, doi:10.4103/2277-9183.102368, 2012.

28 Reuter, M., Buchwitz, M., Hilboll, A., Richter, A., Schneising, O., Hilker, M., Heymann, J.,
29 Bovensmann, H. and Burrows, J. P.: Decreasing emissions of NO_x relative to CO₂ in East Asia
30 inferred from satellite observations, *Nat. Geosci.*, 7(11), 792–795, doi:10.1038/ngeo2257, 2014.

31 Richter, A. and Burrows, J. P.: Tropospheric NO₂ from GOME measurements, *Adv. Sp. Res.*,
32 29(11), 1673–1683, 2002.

33 Richter, A., Burrows, J. P., Nüss, H., Granier, C. and Niemeier, U.: Increase in tropospheric
34 nitrogen dioxide over China observed from space., *Nature*, 437(7055), 129–132,
35 doi:10.1038/nature04092, 2005.

36 Richter, A., Begoin, M., Hilboll, A. and Burrows, J. P.: An improved NO₂ retrieval for the
37 GOME-2 satellite instrument, *Atmos. Meas. Tech.*, 4(6), 1147–1159, doi:10.5194/amt-4-1147-
38 2011, 2011.

39 Richter, A., Hillbol, A. and Burrows, J. P.: Improving S5P NO₂ retrievals, [online] Available
40 from: http://seom.esa.int/atmos2015/page_presentations.php (Accessed 7 March 2016), 2015.

41 Rix, M., Valks, P., Hao, N., Loyola, D., Schlager, H., Huntrieser, H., Flemming, J., Koehler, U.,

1 Schumann, U. and Inness, A.: Volcanic SO₂, BrO and plume height estimations using GOME-2
2 satellite measurements during the eruption of Eyjafjallajökull in May 2010, *J. Geophys. Res.*
3 *Atmos.*, 117(6), doi:10.1029/2011JD016718, 2012.

4 Russell, A. R., Valin, L. C. and Cohen, R. C.: Trends in OMI NO₂ observations over the United
5 States: effects of emission control technology and the economic recession, *Atmos. Chem. Phys.*,
6 12(24), 12197–12209, doi:10.5194/acp-12-12197-2012, 2012.

7 Schmidt, A., Leadbetter, S., Theys, N., Carboni, E., Witham, C. S., Stevenson, J. A., Birch, C.
8 E., Thordarson, T., Turnock, S., Barsotti, S., Delaney, L., Feng, W., Grainger, R. G., Hort, M. C.,
9 Höskuldsson, Á., Ialongo, I., Ilyinskaya, E., Jóhannsson, T., Kenny, P., Mather, T. A., Richards,
10 N. A. D. and Shepherd, J.: Satellite detection, long-range transport, and air quality impacts of
11 volcanic sulfur dioxide from the 2014-2015 flood lava eruption at Bárðarbunga (Iceland), *J.*
12 *Geophys. Res. Atmos.*, 120(18), 9739–9757, doi:10.1002/2015JD023638, 2015.

13 Schneider, P. and Van Der A, R. J.: A global single-sensor analysis of 2002-2011 tropospheric
14 nitrogen dioxide trends observed from space, *J. Geophys. Res. Atmos.*, 117(16),
15 doi:10.1029/2012JD017571, 2012.

16 Schneider, P., Lahoz, W. A. and van der A, R.: Recent satellite-based trends of tropospheric
17 nitrogen dioxide over large urban agglomerations worldwide, *Atmos. Chem. Phys.*, 15(3), 1205–
18 1220, doi:10.5194/acp-15-1205-2015, 2015.

19 Schoeberl, M. R., Douglass, A. R., Hilsenrath, E., Bhartia, P. K., Beer, R., Waters, J. W.,
20 Gunson, M. R., Froidevaux, L., Gille, J. C., Barnett, J. J., Levelt, P. F. and DeCola, P.: Overview
21 of the EOS aura mission, *IEEE Trans. Geosci. Remote Sens.*, 44(5), 1066–1072,
22 doi:10.1109/TGRS.2005.861950, 2006.

23 Schumann, U. and Huntrieser, H.: The global lightning-induced nitrogen oxides source, *Atmos.*
24 *Chem. Phys.*, 7(14), 3823–3907, doi:10.5194/acp-7-3823-2007, 2007.

25 Seftor, C. J., Jaross, G., Kowitt, M., Haken, M., Li, J. and Flynn, L. E.: Postlaunch performance
26 of the Suomi National Polar-orbiting Partnership Ozone Mapping and Profiler Suite (OMPS)
27 nadir sensors, *J. Geophys. Res. Atmos.*, 119(7), 4413–4428, doi:10.1002/2013JD020472, 2014.

28 Seinfeld, J. H. and Pandis, S. N.: *Atmospheric Chemistry and Physics: From Air Pollution to*
29 *Climate Change*, 2nd Edn. 2006, John Wiley & Sons, Hoboken, New Jersey, 2006.

30 Simon, H., Reff, A., Wells, B., Xing, J. and Frank, N.: Ozone trends across the United States
31 over a period of decreasing NO_x and VOC emissions., *Environ. Sci. Technol.*, 49(1), 186–95,
32 doi:10.1021/es504514z, 2015.

33 Smith, S. J., van Aardenne, J., Klimont, Z., Andres, R. J., Volke, A. and Delgado Arias, S.:
34 Anthropogenic sulfur dioxide emissions: 1850–2005, *Atmos. Chem. Phys.*, 11(3), 1101–1116,
35 doi:10.5194/acp-11-1101-2011, 2011.

36 Solomon, P. A., Crumpler, D., Flanagan, J. B., Jayanty, R. K. M., Rickman, E. E. and McDade,
37 C. E.: U.S. national PM_{2.5} Chemical Speciation Monitoring Networks-CSN and IMPROVE:
38 description of networks., *J. Air Waste Manag. Assoc.*, 64(12), 1410–38 [online] Available from:
39 <http://www.ncbi.nlm.nih.gov/pubmed/25562937> (Accessed 7 March 2016), 2014.

40 Stammes, P., Sneep, M., de Haan, J. F., Veefkind, J. P., Wang, P. and Levelt, P. F.: Effective
41 cloud fractions from the Ozone Monitoring Instrument: Theoretical framework and validation, *J.*
42 *Geophys. Res. Atmos.*, 113(16), 1–12, doi:10.1029/2007JD008820, 2008.

1 Stavrakou, T., Müller, J.-F., Boersma, K. F., De Smedt, I. and van der A, R. J.: Assessing the
2 distribution and growth rates of NO_x emission sources by inverting a 10-year record of NO₂
3 satellite columns, *Geophys. Res. Lett.*, 35(10), L10801, doi:10.1029/2008GL033521, 2008.

4 Streets, D. G., Canty, T., Carmichael, G. R., de Foy, B., Dickerson, R. R., Duncan, B. N.,
5 Edwards, D. P., Haynes, J. A., Henze, D. K., Houyoux, M. R., Jacob, D. J., Krotkov, N. A.,
6 Lamsal, L. N., Liu, Y., Lu, Z., Martin, R. V., Pfister, G. G., Pinder, R. W., Salawitch, R. J. and
7 Wecht, K. J.: Emissions estimation from satellite retrievals: A review of current capability,
8 *Atmos. Environ.*, 77, 1011–1042, doi:10.1016/j.atmosenv.2013.05.051, 2013.

9 Theys, N., De Smedt, I., van Gent, J., Danckaert, T., Wang, T., Hendrick, F., Stavrakou, T.,
10 Bauduin, S., Clarisse, L., Li, C., Krotkov, N., Yu, H., Brenot, H. and Van Roozendaal, M.:
11 Sulfur dioxide vertical column DOAS retrievals from the Ozone Monitoring Instrument: Global
12 observations and comparison to ground-based and satellite data, *J. Geophys. Res. Atmos.*,
13 120(6), 2470–2491, doi:10.1002/2014JD022657, 2015.

14 Tian, H., Qiu, P., Cheng, K., Gao, J., Lu, L., Liu, K. and Liu, X.: Current status and future trends
15 of SO₂ and NO_x pollution during the 12th FYP period in Guiyang city of China, *Atmos.*
16 *Environ.*, 69, 273–280, doi:10.1016/j.atmosenv.2012.12.033, 2013.

17 Tong, D. Q., Lamsal, L., Pan, L., Ding, C., Kim, H., Lee, P., Chai, T., Pickering, K. E. and
18 Stajner, I.: Long-term NO_x trends over large cities in the United States during the great
19 recession: Comparison of satellite retrievals, ground observations, and emission inventories,
20 *Atmos. Environ.*, 107, 70–84, doi:10.1016/j.atmosenv.2015.01.035, 2015.

21 Twohy, C. H.: Nitrogenated organic aerosols as cloud condensation nuclei, *Geophys. Res. Lett.*,
22 32(19), L19805, doi:10.1029/2005GL023605, 2005.

23 US Department of Veterans Affairs: Sulfur Fire at Mishraq State Sulfur Mine - Public Health,
24 [online] Available from: <http://www.publichealth.va.gov/exposures/mishraq-sulfur-fire/index.asp>
25 (Accessed 7 March 2016), 2015.

26 US EIA: Coal plants without scrubbers account for a majority of U.S. SO₂ emissions - Today in
27 Energy - U.S. Energy Information Administration (EIA), [online] Available from:
28 <http://www.eia.gov/todayinenergy/detail.cfm?id=4410> (Accessed 7 March 2016), 2010.

29 US EPA: National Emissions Inventory (NEI) Air Pollutant Emissions Trends Data, [online]
30 Available from: <http://www.epa.gov/air-emissions-inventories/national-emissions-inventory>
31 (Accessed 7 March 2016), 2015.

32 US EPA: Criteria Air Pollutants, [online] Available from: [https://www.epa.gov/criteria-air-](https://www.epa.gov/criteria-air-pollutants)
33 [pollutants](https://www.epa.gov/criteria-air-pollutants) (Accessed 7 March 2016), 2016.

34 Valin, L. C., Russell, A. R. and Cohen, R. C.: Variations of OH radical in an urban plume
35 inferred from NO₂ column measurements, *Geophys. Res. Lett.*, 40(9), 1856–1860,
36 doi:10.1002/grl.50267, 2013.

37 Valks, P., Pinardi, G., Richter, A., Lambert, J. C., Hao, N., Loyola, D., Van Roozendaal, M. and
38 Emmadi, S.: Operational total and tropospheric NO₂ column retrieval for GOME-2, *Atmos.*
39 *Meas. Tech.*, 4(7), 1491–1514, doi:10.5194/amt-4-1491-2011, 2011.

40 van der A, R. J., Peters, D. H. M. U., Eskes, H., Boersma, K. F., Van Roozendaal, M., De Smedt,
41 I. and Kelder, H. M.: Detection of the trend and seasonal variation in tropospheric NO₂ over
42 China, *J. Geophys. Res. Atmos.*, 111(12), 1–10, doi:10.1029/2005JD006594, 2006.

1 van der A, R. J., Eskes, H. J., Boersma, K. F., van Noije, T. P. C., Van Roozendaal, M., De
2 Smedt, I., Peters, D. H. M. U. and Meijer, E. W.: Trends, seasonal variability and dominant NO_x
3 source derived from a ten year record of NO₂ measured from space, *J. Geophys. Res.*, 113(D4),
4 D04302, doi:10.1029/2007JD009021, 2008.

5 Vautard, R., Cattiaux, J., Yiou, P., Thépaut, J.-N. and Ciais, P.: Northern Hemisphere
6 atmospheric stilling partly attributed to an increase in surface roughness, *Nat. Geosci.*, 3(11),
7 756–761, doi:10.1038/ngeo979, 2010.

8 Veefkind, J. P., Aben, I., McMullan, K., Förster, H., de Vries, J., Otter, G., Claas, J., Eskes, H. J.,
9 de Haan, J. F., Kleipool, Q., van Weele, M., Hasekamp, O., Hoogeveen, R., Landgraf, J., Snel,
10 R., Tol, P., Ingmann, P., Voors, R., Kruizinga, B., Vink, R., Visser, H. and Levelt, P. F.:
11 TROPOMI on the ESA Sentinel-5 Precursor: A GMES mission for global observations of the
12 atmospheric composition for climate, air quality and ozone layer applications, *Remote Sens.*
13 *Environ.*, 120, 70–83, doi:10.1016/j.rse.2011.09.027, 2012.

14 Vestreng, V., Ntziachristos, L., Semb, a., Reis, S., Isaksen, I. S. a. and Tarrason, L.: Evolution
15 of NO_x emissions in Europe with focus on road transport control measures, , (x), 1503–1520,
16 doi:10.5194/acp-9-1503-2009, 2009.

17 Vinken, G. C. M., Boersma, K. F., van Donkelaar, A. and Zhang, L.: Constraints on ship NO_x
18 emissions in Europe using GEOS-Chem and OMI satellite NO₂ observations, *Atmos. Chem.*
19 *Phys.*, 14(3), 1353–1369, doi:10.5194/acp-14-1353-2014, 2014a.

20 Vinken, G. C. M., Boersma, K. F., Maasakkers, J. D., Adon, M. and Martin, R. V.: Worldwide
21 biogenic soil NO_x emissions inferred from OMI NO₂ observations, *Atmos. Chem. Phys.*, 14(18),
22 10363–10381, doi:10.5194/acp-14-10363-2014, 2014b.

23 Wang, S., Zhang, Q., Martin, R. V., Philip, S., Liu, F., Li, M., Jiang, X. and He, K.: Satellite
24 measurements oversee China’s sulfur dioxide emission reductions from coal-fired power plants,
25 *Environ. Res. Lett.*, 10(11), 114015, doi:10.1088/1748-9326/10/11/114015, 2015.

26 Witte, J. C., Schoeberl, M. R., Douglass, A. R., Gleason, J. F., Krotkov, N. A., Gille, J. C.,
27 Pickering, K. E. and Livesey, N.: Satellite observations of changes in air quality during the 2008
28 Beijing Olympics and Paralympics, *Geophys. Res. Lett.*, 36(17), L17803,
29 doi:10.1029/2009GL039236, 2009.

30 Zhang, Q., Streets, D. G., He, K., Wang, Y., Richter, A., Burrows, J. P., Uno, I., Jang, C. J.,
31 Chen, D., Yao, Z. and Lei, Y.: NO_x emission trends for China, 1995 - 2004: The view from the
32 ground and the view from space, *J. Geophys. Res. Atmos.*, 112(22), doi:10.1029/2007JD008684,
33 2007.

34 Zhang, Q., Streets, D. G. and He, K.: Satellite observations of recent power plant construction in
35 Inner Mongolia, China, *Geophys. Res. Lett.*, 36(15), doi:10.1029/2009GL038984, 2009.

36 Zhang, X.-P. and Cheng, X.-M.: Energy consumption, carbon emissions, and economic growth
37 in China, *Ecol. Econ.*, 68(10), 2706–2712, doi:10.1016/j.ecolecon.2009.05.011, 2009.

38 Zhao, B., Wang, S., Wang, J., Fu, J. S., Liu, T., Xu, J., Fu, X. and Hao, J.: Impact of national
39 NO_x and SO₂ control policies on particulate matter pollution in China, *Atmos. Environ.*, 77,
40 453–463, doi:10.1016/j.atmosenv.2013.05.012, 2013.

41 Zhou, Y., Brunner, D., Boersma, K. F., Dirksen, R. and Wang, P.: An improved tropospheric
42 NO₂ retrieval for OMI observations in the vicinity of mountainous terrain, *Atmos. Meas. Tech.*,

1 2(2), 401–416, doi:10.5194/amt-2-401-2009, 2009.
2 Zhou, Y., Brunner, D., Hueglin, C., Henne, S. and Staehelin, J.: Changes in OMI tropospheric
3 NO₂ columns over Europe from 2004 to 2009 and the influence of meteorological variability,
4 Atmos. Environ., 46, 482–495, doi:10.1016/j.atmosenv.2011.09.024, 2012.
5 Zyrichidou, I., Koukouli, M. E., Balis, D. S., Kioutsioukis, I., Poupkou, A., Katragkou, E.,
6 Melas, D., Boersma, K. F. and van Roozendaal, M.: Evaluation of high resolution simulated and
7 OMI retrieved tropospheric NO₂ column densities over Southeastern Europe, Atmos. Res., 122,
8 55–66, doi:10.1016/j.atmosres.2012.10.028, 2013.
9
10

1

2

3 **Table A1 Filtering transient volcanic clouds**

Region	Threshold (DU)	Days excluded (2005-2014)
Eastern US	5	97
Eastern Europe	8	72
Eastern China	10	71
India	8	58
Middle East	8	10

4

1

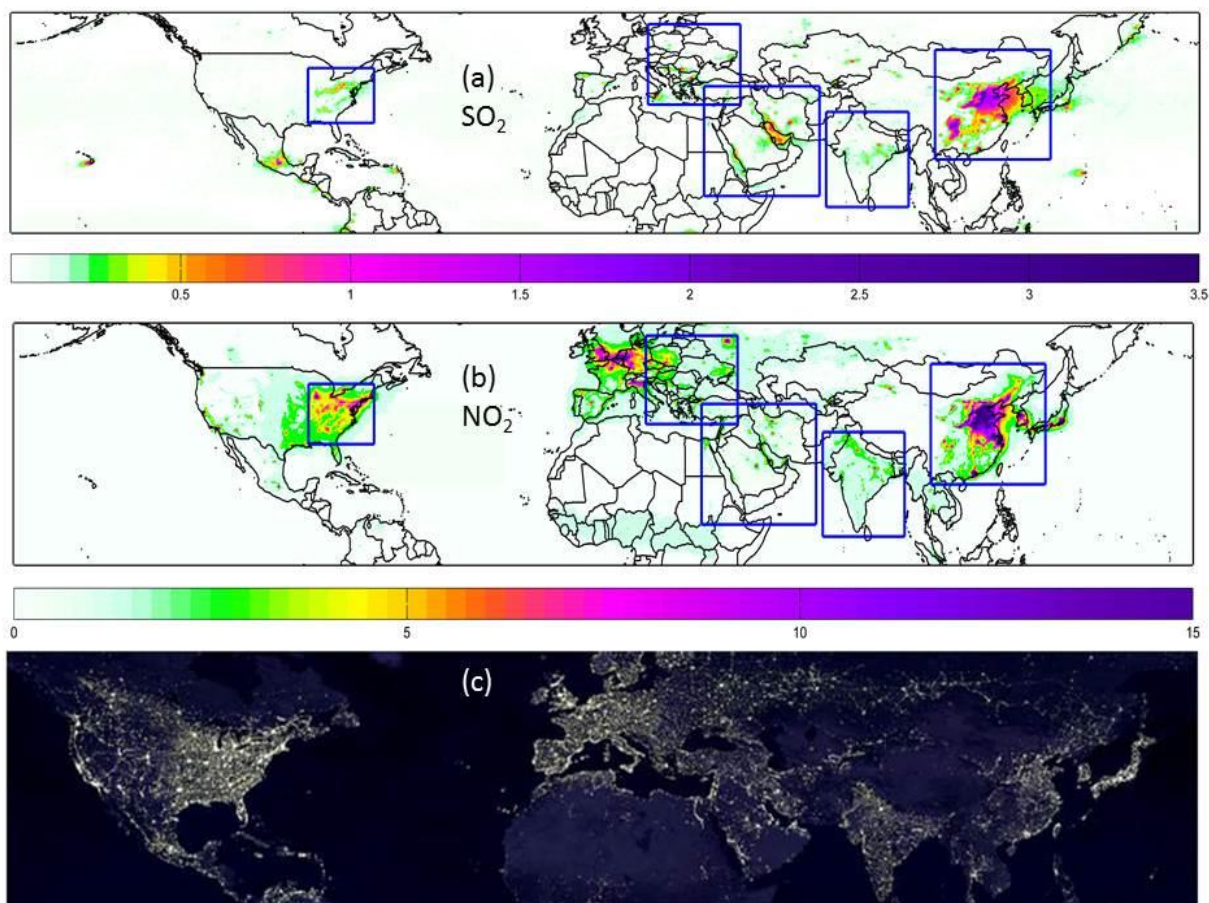


Figure 1. OMI-derived maps of PBL SO₂ in Dobson Units [DU] (a) and tropospheric NO₂ columns in [10¹⁵ molecules/cm²] (b) for 2005-2007 show enhanced pollution levels around major cities and industrial centers, seen also in the “Earth at Night” (city lights) map (c), courtesy of Aura EPO team.

2

3

4

5

1

2 F2

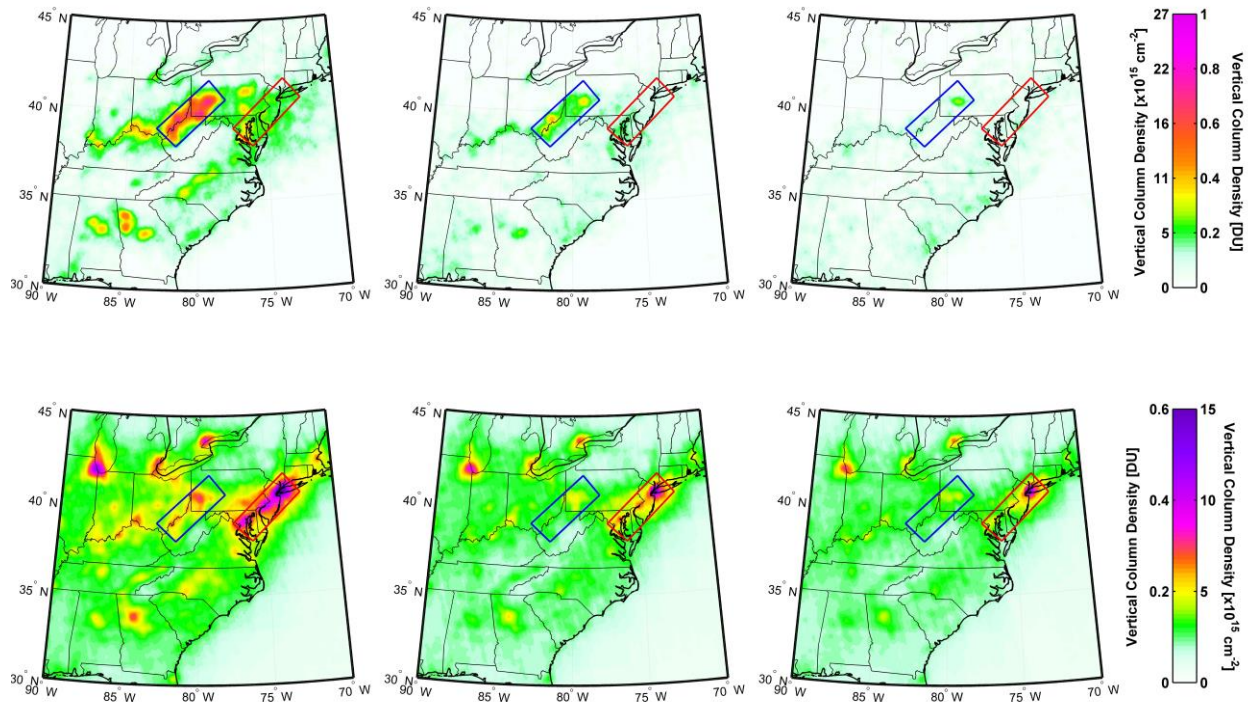


Figure 2. 3-year average OMI SO₂ (top) and tropospheric NO₂ (bottom) regional maps over eastern US for 3 periods: 2005-2007 (left), 2009-2011 (middle) and 2013-2015 (right). Blue box outlines Ohio River Valley and SW Pennsylvania (ORV) region with largest SO₂ emissions from coal-fired power plants. Red box outlines megalopolis from Washington, DC to New York along the I-95 interstate highway (I-95 corridor) with largest NO₂ from mobile sources.

3

4

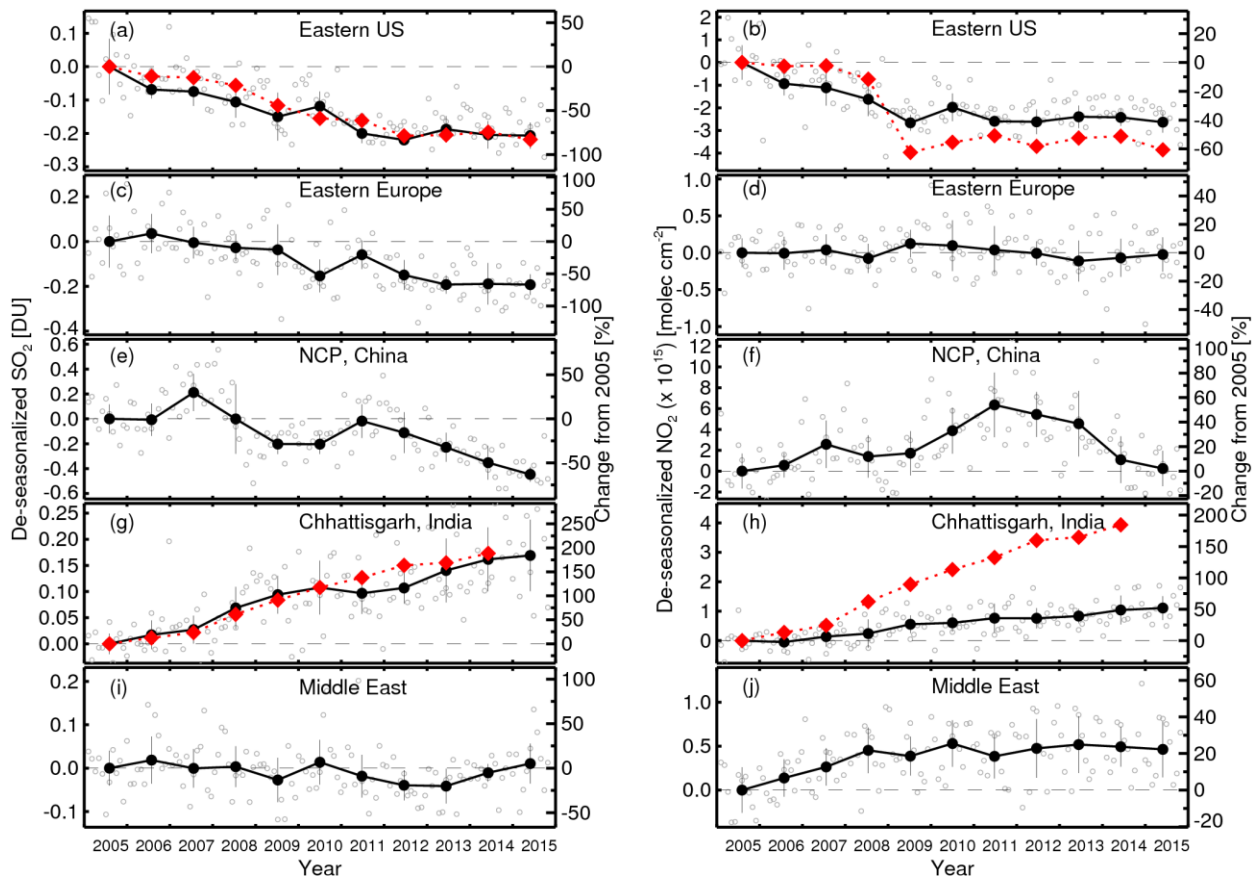


Figure 3. Relative changes (compared to 2005) in OMI PBL SO_2 columns (left) and tropospheric NO_2 columns (right) over 5 world's most polluted regions: (a) and (b): Ohio River Valley and southwestern Pennsylvania (ORV) in eastern US (ORV - blue box in Fig. 2); (c) and (d): Maritsa Iztok Power Plants in Bulgaria (blue box in Fig. 4); (e) and (f): North China Plain (NCP - blue box in Fig.5); (g) and (h): NE India (blue box in Fig. 6); (i) and (j): Persian Gulf (blue box in Fig. 7). Gray circles show de-seasonalized monthly columns (see details in Appendix B). Black filled circles show annual means. Vertical bars show standard deviations. Red diamonds show bottom-up emission estimates for power plants in ORV and from coal-fired power plants in NE India (Chhattisgarh and Odisha region – blue box in Fig. 4).

1

2

3

1

2 F4

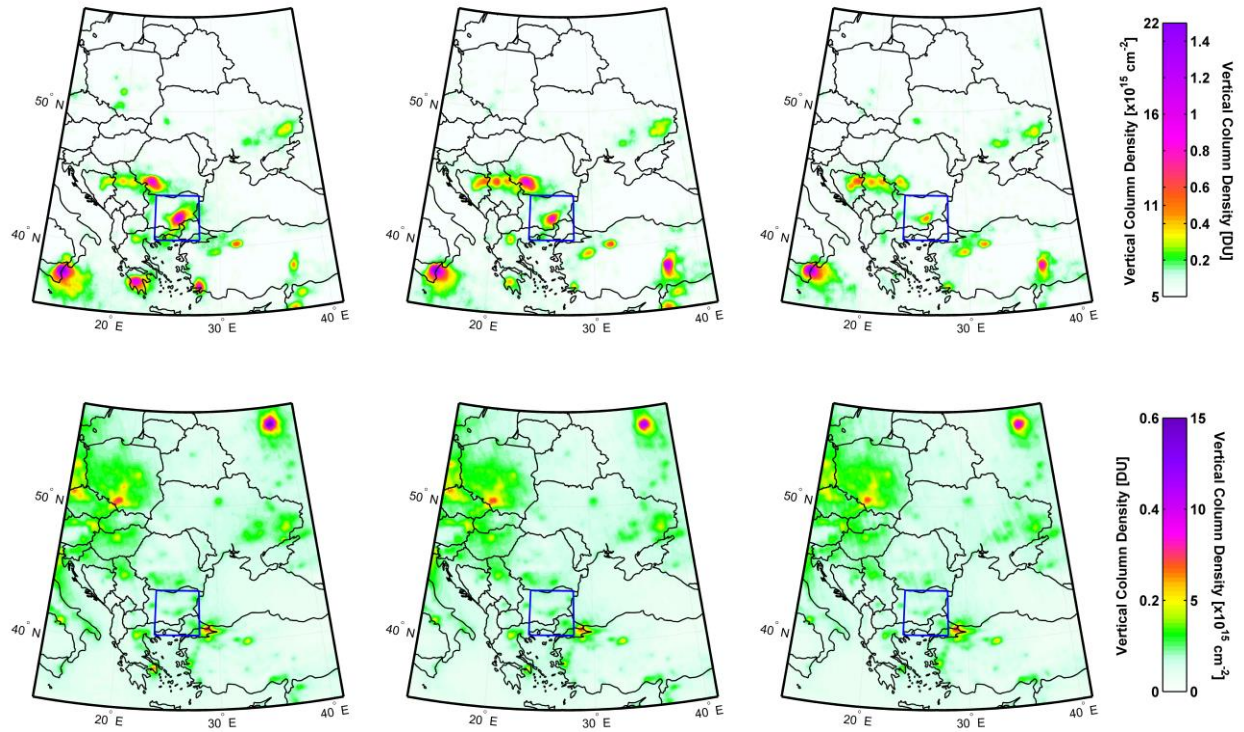


Figure 4: Same as Fig. 2, but for Eastern Europe. The largest SO₂ source in the domain is the Etna volcano in Sicily, Italy. The blue box is centered on SO₂ polluted area around Maritsa Iztok coal mining region and the largest coal-fired power plants in southeastern Bulgaria.

3

4

5

6

7

8

1

2

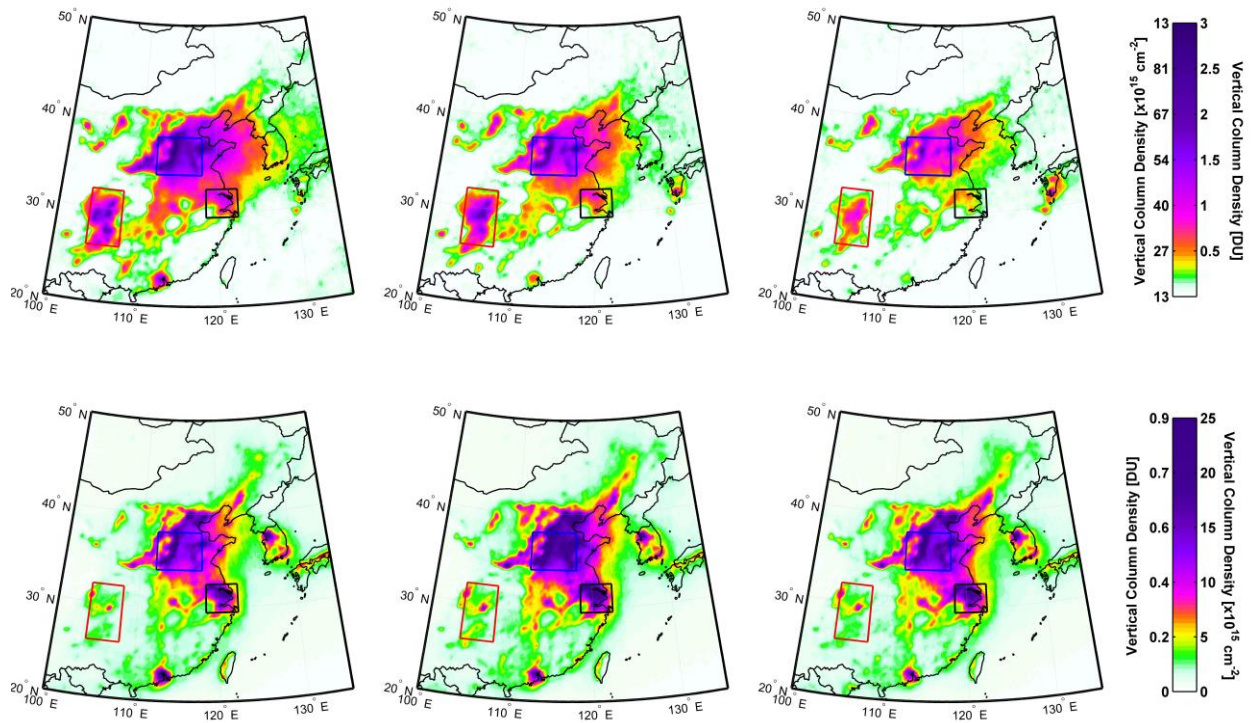


Figure 5. Similar to Figure 2 but for Eastern China. Blue box outlines North China Plane (NCP) also represented in Fig.3, red box - Sichuan Basin (SB) and black box represent Yangtze River Delta (YRD). The boxes are also shown in Fig. S1, S3 and S4.

3

4

5

6 F6

7

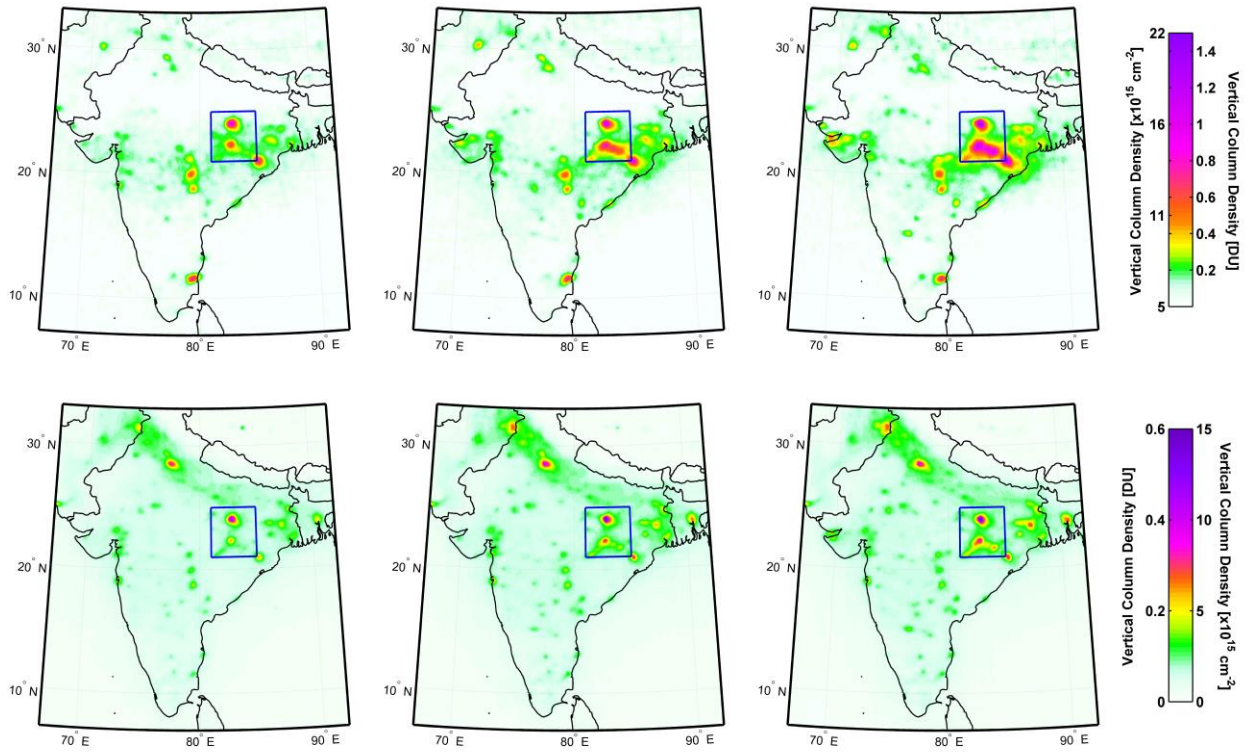


Figure 6. Similar to Fig. 2 but for India. Blue box outlines industrial regions in Chhattisgarh and Odisha, one of India's most active areas in terms of building new coal-fired power plants. The region is shown in Fig.3.

1

2

3

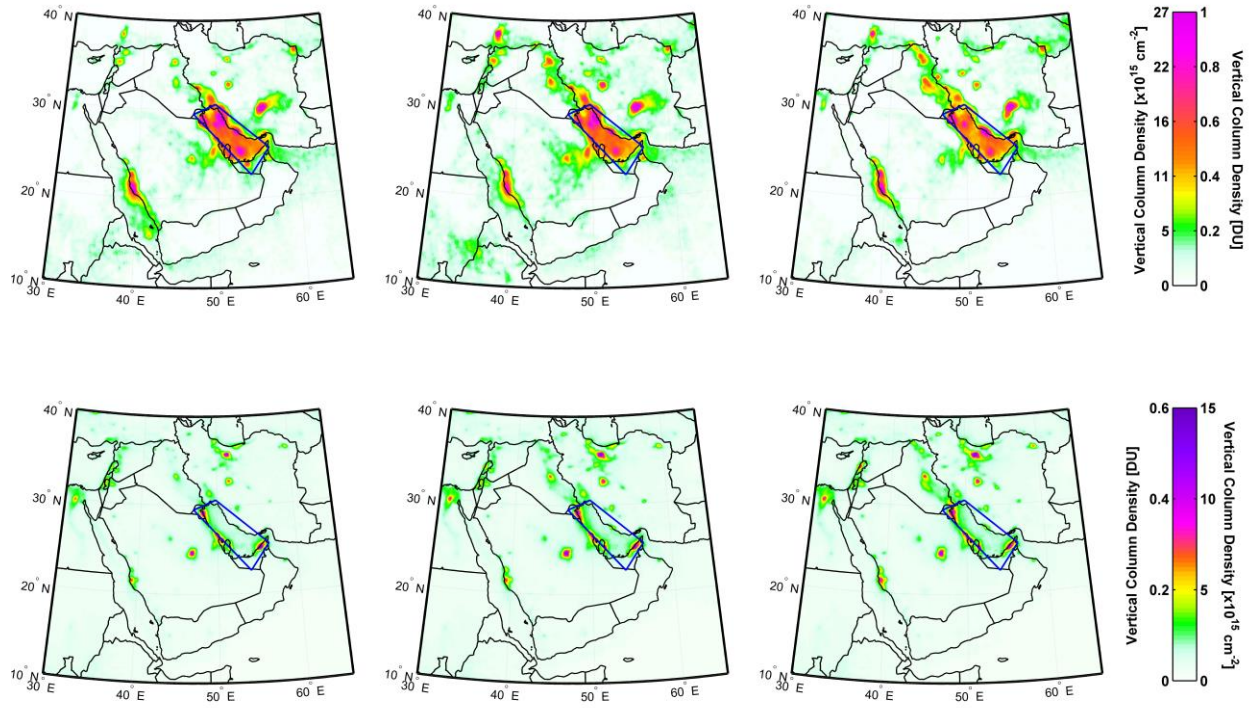


Figure 7. Similar to Fig. 2 but for the Middle East. Blue box outlines Persian Gulf region with high SO₂ and NO₂ levels due to oil and gas operations.

1

2

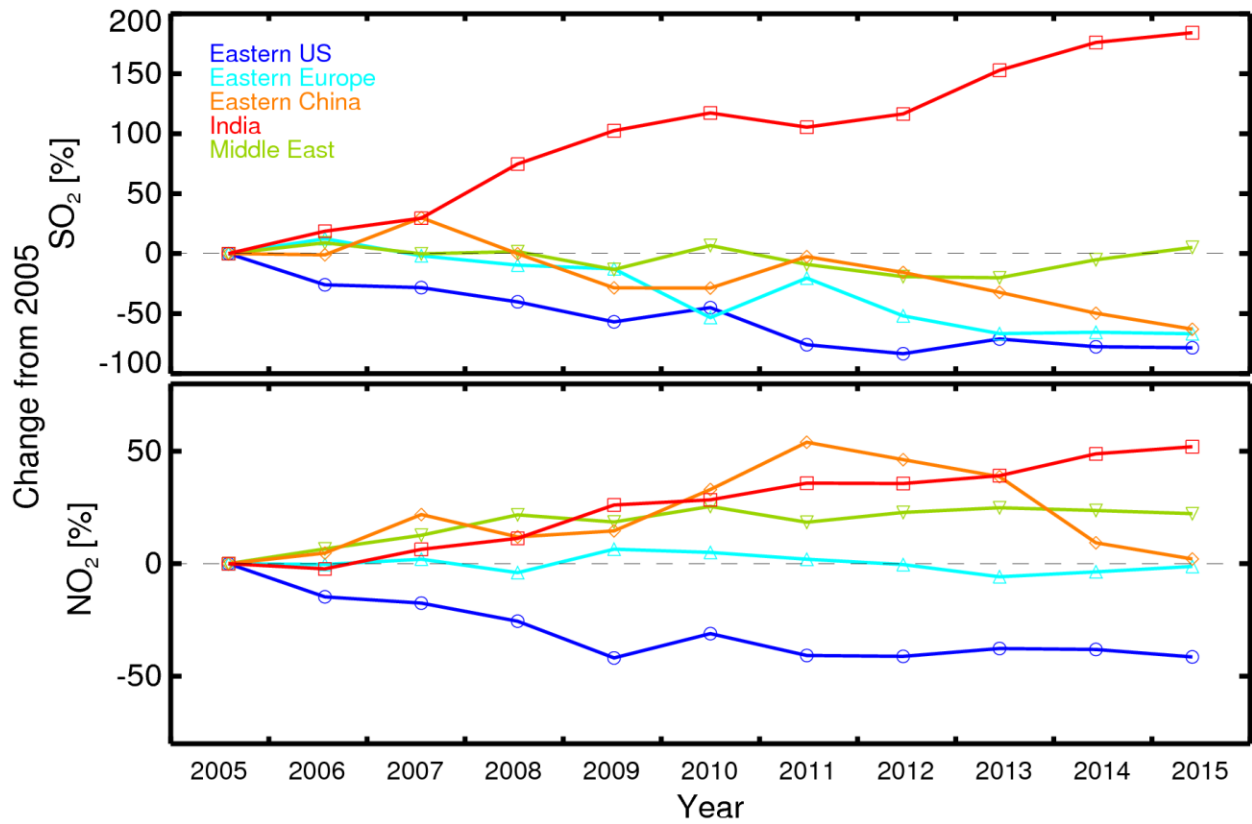


Figure 8. Percent change in OMI annual average columns since 2005: SO₂ (top) and NO₂ (bottom) over the world's most polluted regions discussed in this study.